

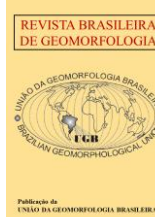


<https://rbgeomorfologia.org.br/>
ISSN 2236-5664

Revista Brasileira de Geomorfologia

v. 26, n° 1 (2025)

<http://dx.doi.org/10.20502/rbgeomorfologia.v26i1.2648>



Artigo de Pesquisa

Sedimentary characterization of coastal environments on Deception Island, Maritime Antarctica

Caracterização sedimentar de ambientes costeiros da Ilha Deception, Antártica Marítima

Diego Augusto Portella¹, Rosemary Vieira², Vanessa C. Costa³ e João Paulo S. Felizardo⁴

¹ Universidade Federal Fluminense, Geografia, Niterói, Brasil. daugusto@id.uff.br

ORCID: <https://orcid.org/0000-0001-5650-8004>

² Universidade Federal Fluminense, Geografia, Niterói, Brasil. rosemaryvieira@id.uff.br

ORCID: <https://orcid.org/0000-0003-0312-289>

³ Universidade Federal Fluminense, Geografia, Niterói, Brasil. vanessacosta@id.uff.br

ORCID: <https://orcid.org/0000-0003-4909-5365>

⁴ Universidade Federal Fluminense, Física, Niterói, Brasil. joapaulosafelizardo@gmail.com

ORCID: <https://orcid.org/0000-0001-6579-7071>

Recebido: 29/11/2024; Aceito: 21/03/2025; Publicado: 03/04/2025

Abstract: Deception Island, situated in the South Shetland Archipelago, Maritime Antarctica, has unique characteristics such as a young and active stratovolcano, which dates back approximately 0.75 Ma. Recently, the island has witnessed glacier retreat, leading to more frequent occurrences of ice-free areas with exposed soil. This phenomenon highlights the intricate interactions between volcanic activity and regional climate warming, reflecting in the formation of the sedimentation environment. This study focuses on the sedimentary characteristics of four subaerial profiles distributed along coastal areas. Sediment samples were collected during the OPERANTAR XXXVI expedition, and underwent a range of analyses including granulometric, morphoscopic, geochemical, isotopic and statistical examinations. The granulometric and morphoscopic analyses suggest that sediments are transported and reworked over relatively short distances from their original source, reflecting rapid sedimentation processes. Iron (Fe) was identified as the most abundant element, likely linked to both tephra deposits from volcanic activity and the early stages of chemical weathering. The isotopic analyses suggest contributions from both local (autochthonous) and distant (allochthonous) sources, primarily involving Antarctic lichens and animal excrement, which are transported by meltwater flows. In conclusion, the sedimentation dynamics on Deception Island are primarily influenced by the volcanic eruptions that occurred between 1967 and 1970. However, glacial and periglacial processes are significant as well, with meltwater flows, liquid precipitation and sediments contributions from glaciers and permafrost, playing a critical role in developing fluvio-glacial deposits in the region. This study enhances the understanding of the complex environmental interactions at Deception Island in the context of ongoing climate change.

Keywords: Vulcanism; Sedimentation; Environmental changes; Antarctica

Resumo: A ilha Deception localizada no arquipélago das Shetland do Sul, Antártica Marítima, apresenta características únicas por ser um estratovulcão jovem e ativo com uma idade de aproximadamente 0,75 Ma e por vivenciar retração nas geleiras com evidências cada vez mais frequentes de áreas de solo exposto. Sendo assim, as interações entre os processos de vulcanismo e de aquecimento climático regional, oriundo das mudanças ambientais globais, refletem na formação do ambiente sedimentação. Dessa forma, o presente trabalho teve como objetivo realizar uma caracterização sedimentar de perfis distribuídos em quatro ambientes costeiros da ilha Deception. Foram realizadas análises granulométricas, morfoscópicas, geoquímicas, isotópicas e

estatísticas em amostras de sedimentos terrestres durante a OPERANTAR XXXVI (2017/2018). As análises granulométricas e morfológicas indicam uma menor distância para transporte e retrabalhamento das amostras desde sua área de origem, além da rápida sedimentação das partículas. As amostras apresentaram o Fe como o elemento em maior quantidade, o que pode estar associado a depósitos de tephra, além da ação do intemperismo químico, ainda que incipiente. As análises isotópicas sugeriram contribuições autóctones e alóctones, principalmente de líquens antárticos e excrementos de animais, transportados por fluxos de água de degelo. Diante disso, conclui-se que a dinâmica atual de sedimentação da ilha Deception seja controlada majoritariamente pelas últimas atividades vulcânicas no período 1967-1970, embora com participação dos processos glaciais e periglaciais a partir de fluxos de água de fusão, de precipitações líquidas e de sedimentos das geleiras e do permafrost, que contribuem para a formação de depósitos fluvio-glaciais na região.

Palavras-chave: Vulcanismo; Sedimentação; Mudanças ambientais, Antártica.

1. Introduction

The Maritime Antarctic, encompassing the west and north coasts of the Antarctic Peninsula and the offshore islands, is notably susceptible to climate change. According to the Intergovernmental Panel on Climate Change (IPCC, 2021) the Antarctic Peninsula region has been experiencing increasing temperatures, raising concerns within the scientific community.

Deception Island, situated in the Bransfield Strait south of the South Shetland Islands, is a young stratovolcano approximately 0.75 Ma old. It is part of a series of volcanoes that developed along the rift axis of the Bransfield Strait (GRACIA et al., 1997; BARALDO; RINALDI, 2000).

The island's unique features, including glaciers, ice-free areas with permafrost, and active volcanism, make it a relevant site for studying environmental transformations in the context of rising temperatures, increased liquid precipitation, and deglaciation. Previous sedimentological studies on Deception Island, particularly in its ice-free areas, have focused on aspects, such as igneous petrology (KELLER and FISK, 2002; FERREIRA et al., 2015), glacial and periglacial processes, soil formation, and permafrost dynamics (BALDWIN and SMITH, 2003; VIEIRA et al., 2008; GOYANES et al., 2014; MUNIZ et al., 2018).

The changing landscape of Deception Island, as noted by Muniz et al. (2018), poses significant questions regarding its landscape transformation and consequent sedimentation processes. With deglaciation driven by both volcanic activity and regional warming in the South Shetland region (TURNER et al., 2014; ABRAM et al., 2016), there is a pressing need to explore the interconnectedness of these processes. The interplay between glacier melt, permafrost changes, and sediment dynamics remains underexplored, warranting a more detailed investigation (MUNIZ et al., 2018).

In light of the rising temperatures on the Antarctic Peninsula, it is crucial to discern whether sedimentation on Deception Island is predominantly influenced by volcanic activity or by the effects of regional increased air temperatures.

This study aims to assess sedimentary environment through an analysis of subaerial sediments from ice-free coastal areas of Deception Island, including South Whalers, Whalers Bay, Pendulum Cove and Cross Hill. This analysis will contribute insights into the dynamics of the island's volcano-glacial landscape and enhance our understanding of its evolving ecological and geomorphological framework.

2. Area of study

Deception Island (Figure 1) is an active volcano whose crater has been flooded by seawater. The island is part of a chain of volcanoes (such as Penguin and Brindgeman Islands) that developed along the rift axis of the Bransfield Strait, with fumaroles and geothermal sources reaching temperatures up to 70°C (GRACIA et al., 1997; BARALDO; RINALDI, 2000).

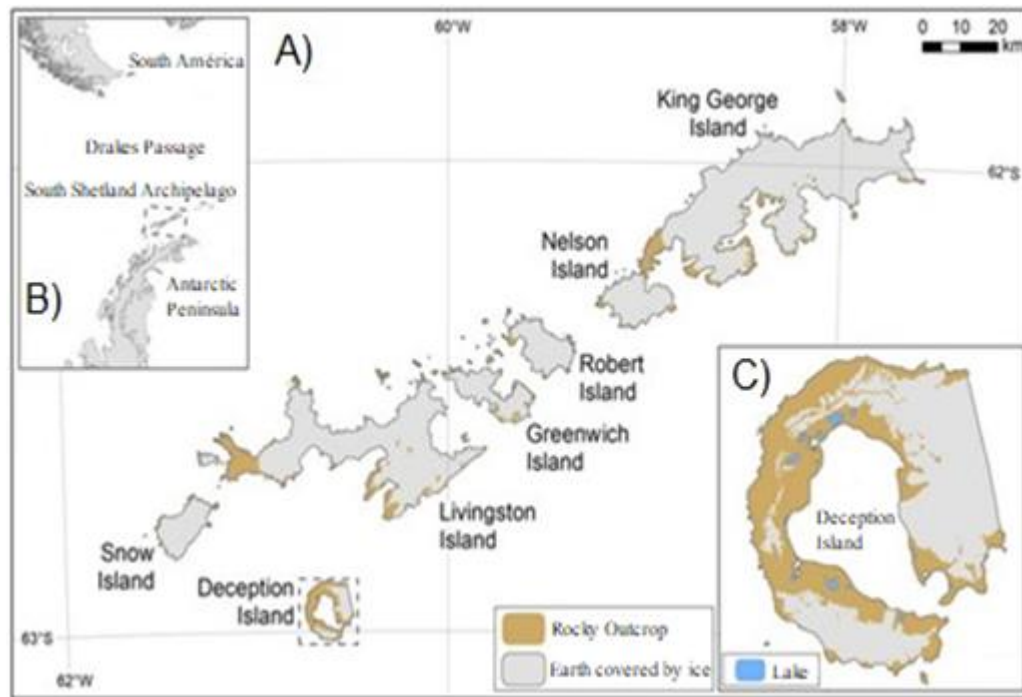


Figure 1. Location Map of Deception Island. A) Maritime Antarctica, B) South Shetland Islands, C) Deception Island.

Source: CARVALHO-SILVA et al. (2021).

The central caldera's collapse led to the inundation of its basin, forming Porto Foster Bay, which contributes to the island's distinctive horseshoe shape (BARTOLINI et al, 2014). The caldera features approximately 25 km of submerged base and around 15 km of exposed land. This area is known for its volcanic activity, including significant eruptions in 1967, 1969, and 1970, that resulted in the destruction of the scientific bases located there (BARTOLINI et al., 2014).

Historical records indicate heightened volcanic activity during the years 1818-1828, 1906-1912, followed by a prolonged dormancy from 1912 to 1967, when explosive eruptions reoccurred (GEYER et al., 2017). Further volcanic unrest was reported in 1992, 1999 and again in 2014-2015, underscoring the island's ongoing volcanic nature (GEYER et al., 2017; HOPFENBLATT et al., 2021). Recent geophysical surveys conducted by Leitão et al. (2016), have mapped new underwater volcanic cones in Porto Foster Bay, reinforcing the presence of active volcanic processes and the potential for future eruptions.

Geologically, the rocks and deposits of Deception Island are categorized into three phases: pre-caldera, syn-caldera and post-caldera. The "Porto Foster" geological group includes the pre- and sin-caldera deposits while the "Monte Pound" geological group consists of the post-caldera deposits (BARALDO; RINALDI, 2000; SMELLIE, 2002).

Volcanic eruptions on Deception Island are notably characterized by explosive hydrovolcanic interactions. These occurs when magma interacts explosively with water, which may be found in underground water tables, shallow subsurface layers, saturated sediments, seawater from Porto Foster Bay or glacial melt (PEDRAZZI et al., 2018). As a result, eruptions of small volume pose significant hazards, particularly when they happen in flooded coastal areas or near ice masses (PEDRAZZI et al., 2018).

The island's morphology is primarily shaped by volcanic activity, alongside processes including glacial, periglacial and tectonic influences (LÓPEZ-MARTÍNEZ; SERRANO, 2002; MAESTRO et al., 2007). Deception Island exhibits paraglacial features, which are sedimentary deposits found in previously glaciated areas and continue to be shaped by geomorphological processes linked to post-glacial adjustment. This includes pyroclastic materials from volcanic eruptions that cover extensive portions of the island (BALLANTYNE, 2002). Additionally, many glaciers on the island are covered by layers of ash and volcanic debris, with some areas featuring a thin deposit layer ranging from 30 to 90 cm thick (SMELLIE, 2002; VIEIRA et al., 2008).

Along the shores of Porto Foster Bay, sandy sediments often accumulate in meltwater channels. This type of sediment is particularly abundant in Whalers Bay and Cross Hill (Figure 2). The glaciogenic processes, notably the

meltwater through these channels, play an important role in influencing erosion and sediment accumulation in the area. Additionally, volcanic activity contributes to the transport of these sediments (SMELLIE, 2001; MUNIZ et al., 2018).

3. Materials and Methods

3.1 Sampling

Samples of terrestrial profiles were collected during the XXXVI Antarctic Operation (2017/2018), supported by the Brazilian Antarctic Program (PROANTAR) and the National Institute of Cryosphere Science and Technology (INCT Criosfera). Figure 2 illustrates the location map of Deception Island, highlighting the sampling points.

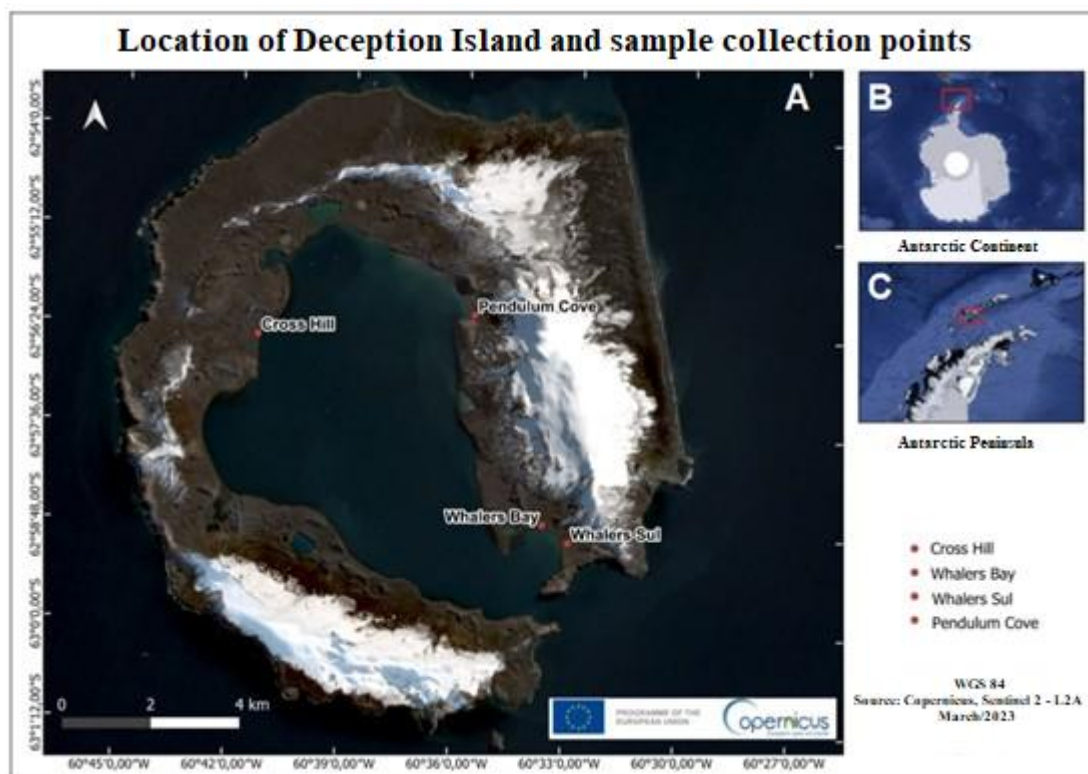


Figure 2. Geographic location of the study area showing: (A) Aerial photograph of Deception Island and sample collection points; (B) Location of the South Shetland Islands in the Antarctic continent; (C) Location of Deception Island Photograph. Source: European Union, Copernicus Sentinel 2 (2023).

Sediment samples were collected in sites near the shoreline (Figure 3) at maximum elevation of 6 meters above sea level, where no snowmelt flow channels were observed. The sediments were sampled from pits excavated to a depth of 85 to 100 cm, with samples taken at every 10 cm layer. This depth range was selected based on previous studies (FAO, 2006), which indicate that it corresponds to the limit of permafrost development, directly influencing soil characteristics in the region.

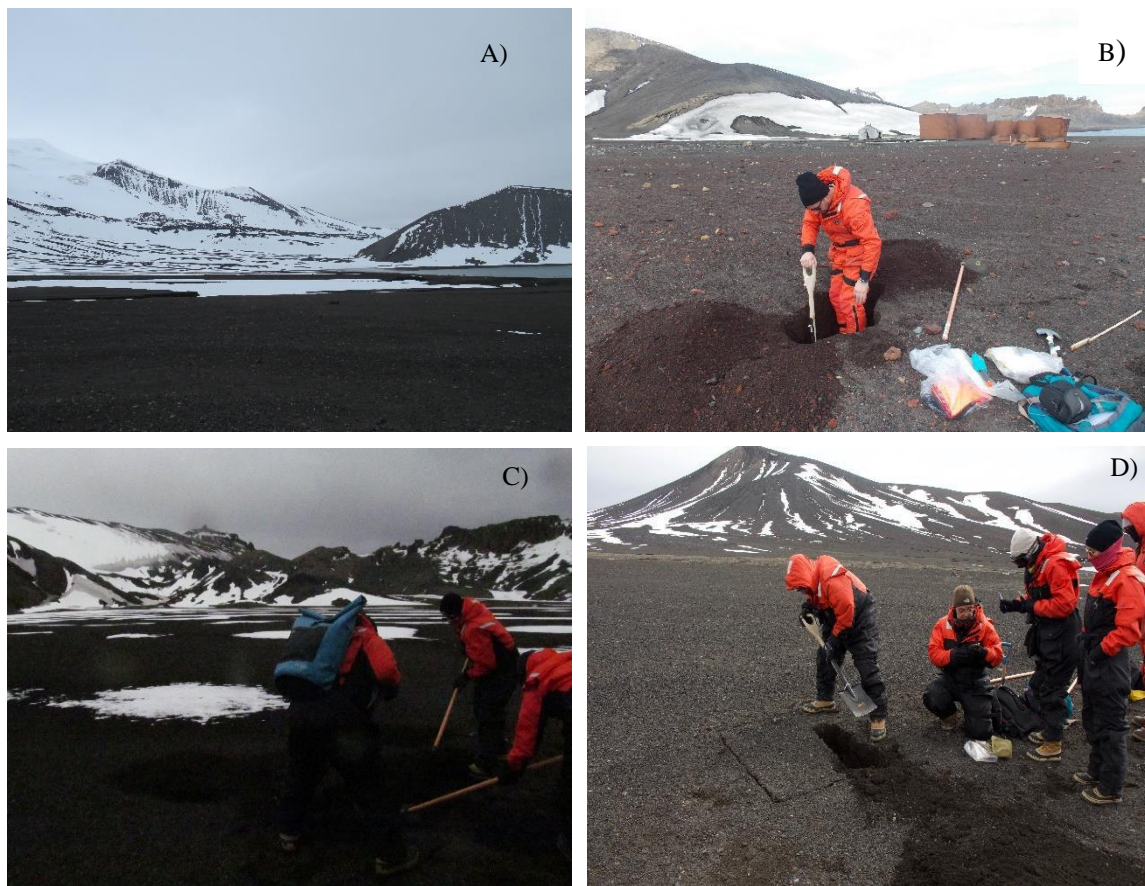


Figure 3. Sampling points: A) Cross Hill, B) Whalers Bay, C) South Whalers, D) Pendulum Cove. Photos: Authors.

The Pendulum Cove samples were collected in a flat area near the shoreline, surrounded by slopes. Meltwater flows were observed nearby, though not at the sampling site. The site is characterized by the presence of dark gray “heated ground” and small patches of vegetation along the coast, including moss and lichen. In the field, a temperature of 4°C was recorded in the surface layer of the profile, while at a depth of 100 cm, the temperature reached 20°C.

3.2 Granulometric analysis

The granulometric analysis followed the classification system of the Classification System of the Brazilian Association of Technical Standards (ABNT, 1995). Coarser samples (> 63 µm) were analyzed using a CAMSIZER particle analyzer, while the fine sediment samples (< 63 µm) were reserved for the Malvern laser granulometer. Notably, at Pendulum Cove, at the 80 and 100 cm layers, no fine fraction was found, as the entire sample was retained in the 63 µm sieve mesh.

The coarse fraction (> 63 µm) was analyzed dry using a Retsch CAMSIZER P4 laser particle analyzer, capable of measuring sediment particles ranging from 20 to 30,000 µm. The fine fraction (muddy sediments) was analyzed wet with a Mastersizer Hydro 2000 G laser granulometer (Malvern Instrument), with sieve openings ranging from 0.3 to 56 µm. This analysis was conducted at the Institute of Geosciences, Fluminense Federal University (UFF).

The statistical parameters obtained were processed using Gradistat V8 software, developed by Blott and Pye (2001). This software operates within Microsoft Excel and applies the statistical methods of Folk and Ward (1957).

3.3 Particle size analysis

The coarse fraction sediment ($> 63 \mu\text{m}$) was first sieved through a 2 mm mesh, after which approximately 50 of the largest clasts were selected for morphoscopic analysis using a binocular microscope and a digital caliper. The objective was to identify specific characteristics in the samples, such as size, shape, and roundness. Roundness was assessed visually under a binocular microscope, following the criteria established by Benn; Ballantyne (1994), based on the Powers scale (1953, and later modified by HUBBARD; GLASSER, 2005). This method allows for inferences about the temporal distinction between erosion, transport and deposition processes (LUKAS et al., 2013).

Additionally, the selected clasts were analyzed using a digital caliper at the Laboratory of Sedimentary and Environmental Processes (LAPSA) of the Geosciences Institute, Fluminense Federal University. This analysis aimed to determine the relative sizes of the three orthogonal axes: a (longest), b (intermediate), c (shortest). From these measurements, the ratio $c/a \leq 0.4$ (EVANS; BENN, 2004), was calculated generating the C40 Index, which helps to distinguish between actively and passively transported sediments, as well as estimating transport distances. The percentages of very angular (VA) and angular (A) clasts were also determined to calculate the RA Index. Furthermore, the RWR Index (percentage of rounded and well-rounded clasts) was assessed according to the methodology proposed by Evans; Benn (2004) and by Lukas et al. (2013). The charts were generated using Golden Software Grapher.

3.4 Chemical analysis

X-ray fluorescence (XRF) analysis was performed on sediments from the silt and clay fractions ($< 0.03 \text{ mm}$), which were macerated. The analyses were conducted using an Epsilon 1 Malvern Panalytical energy-dispersive analyzer at the Laboratory of Sedimentology, Institute of Geosciences (Fluminense Federal University). The Epsilon 1 system consists of an integrated spectrometer with an X-ray tube featuring Ag and Be cathodes, as well as a computer equipped with Omnian analytical software, which adjusts the analysis parameters according to the sample type (GALVÃO, 2021).

The proportions of major chemical elements, along with the percentage by weight of their corresponding oxides, were used to calculate the Chemical Index of Alteration (CIA) (NESBITT; YOUNG, 1982) and the Plagioclase Index of Alteration (PIA) (FEDO et al., 2012), serving as paleoclimatic and paleoenvironmental proxies. The CIA is interpreted as a measure of the extent of feldspar conversion into clay minerals, while the PIA follows values derived from the CIA formula. The indices were calculated using the mathematical equations proposed by Nesbitt; Young (1982):

$$\text{CIA} = (\text{Al}_2\text{O}_3 / (\text{Al}_2\text{O}_3 + \text{CaO} + \text{Na}_2\text{O} + \text{K}_2\text{O})) \times 100.$$

$$\text{PIA} = [(\text{Al}_2\text{O}_3 - \text{K}_2\text{O}) / (\text{Al}_2\text{O}_3 + \text{CaO} + \text{Na}_2\text{O} - \text{K}_2\text{O})] \times 100: (2)$$

Where oxides are expressed as molar ratios (FEDO et al., 2012):

$$\text{Moles Al}_2\text{O}_3 = \% \text{ Al}_2\text{O}_3 / 101,96$$

$$\text{Moles CaO} = \% \text{ CaO} / 56,08$$

$$\text{Moles NaO} = \% \text{ NaO} / 61,98$$

Values close to 100 for both indices suggest intense chemical weathering, whereas values below 55 indicate the absence or incipience of chemical weathering.

3.5 Isotopic analysis

Carbon and nitrogen isotopic analysis was conducted to enhance the understanding of soil organic matter. Given the scarcity of vegetation in the region, characterizing the organic content is essential for understanding soil dynamics and identifying the source material of the samples.

For this procedure, sediments from the silt and clay fraction (size $< 0.06 \text{ mm}$) were used. The decarbonation test, following the GIBBS protocol (2010) was applied prior to isotopic analysis. However, since the sediment samples are of terrigenous origin, no carbonates were detected.

Stable isotopes analysis was performed using Isotope Ratio Mass Spectrometry (IRMS) at the Laboratory of Radioecology and Environmental Changes (LARA), Physics Institute, Federal Fluminense University. The Analysis was conducted with a FlashEA2000 elemental analyzer equipped with an automatic MAS200R sampler (32-sample capacity), coupled to a DELTA V Advantage IRMS via a ConFlo IV universal interface. Total Organic Carbon (TOC) values were obtained.

3.6 Statistical Analysis

Pearson's correlation was applied to assess the relationship between granulometry and geochemical data (elements, oxides, and CIA) across profile layers. Pearson's linear correlation coefficient ("r") was determined with a significance level ("p"), calculated using Student's "t"-test, which indicates the probability of a non-existent correlation. The critical value adopted as a standard in the Paleontological Statistics (PAST) 4.01 software was $p < 0.05$, following the algorithms of Press et al. (1992). When correlating layer depth (cm) with the variables (expressed as percentages), a logarithmic transformation was applied beforehand.

Principal Components Analysis (PCA) was performed as a variable transformation technique to identify linear components of correlated variables that capture the maximum variance (LANDIN, 2011; HAMMER, 20212). The variance-covariance matrix was used as input, since all variables were expressed in the same units (percentages) in this study. PCA was applied to further explore the relationship among the eight major chemical elements, sampling locations and profile layers. Multivariate analysis was conducted using the free software Paleontological Statistics (PAST) 4.01.

4. Results

This section presents the results of the distinct analyses conducted on the profiles. First, the morphoscopic characteristics and physical properties of the sedimentary profiles are described. Next, data on chemical elements and weathering processes are presented. This is followed by the results of the isotopic analysis. Finally, the data obtained from the statistical analysis are displayed.

4.1. Morphology and physical properties of profiles

The soil particle size analyses from Pendulum Cove, Whalers Bay, South Whalers and Cross Hill are presented in Figure 4. In Pendulum Cove, the sand fraction is the most abundant throughout the profile (Figure 4A), followed by gravel, silt and clay. The lowest sand percentage is found at the surface (42.7%), while the highest occurs at the 10 cm layer (78.8%), which also corresponds to the lowest gravel fraction (19.8%). Conversely, the highest gravel fraction (56.5%) is observed at the 100 cm layer. The percentage of silt and clay fractions shows little variation, with silt ranging from 1.15% at the 70 cm (lowest concentration) to 3.6% at 50 cm (highest concentration). The clay fraction varies between 0.1% (70 cm) and 0.4% (50 cm). As previously noted, no significant amounts of silt or clay were detected at the 80 cm and 100 cm layers.

The Whalers Bay profile (Figure 4B) differs from the others, as it has a higher percentage of gravel compared to sand, silt and clay. The gravel fraction reaches its peak at the 75 cm layer (72.3%), where the sand fraction is at its lowest (23.3%). In contrast, the lowest gravel percentage (41.0%) is found at the 15 cm layer, coinciding with the highest sand content (52.9%). Silt and clay fractions exhibit minimal variation, with silt ranging from 3.2% at 65 cm (lowest) to 6.8% at 0.5 cm (highest). Similarly, clay content varies between 0.1% (65 cm) and 0.3% (0.5 cm).

The granulometric profile of South Whalers (Figure 4C) shows the sand fraction is the most abundant, followed by gravel, silt and clay. The highest sand percentage is observed at the 10 cm layer (78.4%), which also corresponds to the lowest gravel fraction (15.9%). Conversely, the lowest sand content (51.8%) is found at the 30 cm layer, where the highest gravel fraction (42.4%) occurs. The silt fraction varies between 5.4% at the 40 cm layer and 17.4% at the surface. The clay fraction remains relatively stable, ranging from 0.3% (10, 30, and 40 cm layers) to 1.2% at 50 cm layer.

The grain size profile of Cross Hill (Figure 4D) is also dominated by the sand fraction, followed by gravel, silt, and clay. The lowest percentage (49.0%) occurs at the 50 cm layer, where the gravel fraction reaches its peak (43.1%). In contrast, the highest sand content (81%) is observed at the 80 cm layer, which also corresponds to the lowest gravel fraction (15.2%). Silt content varies between 2.4% at 60 cm and 14.1% at the surface. The clay fraction shows minimal variation, ranging from 0.1% at the 60 cm layer to 1.1% at 20 cm layer.

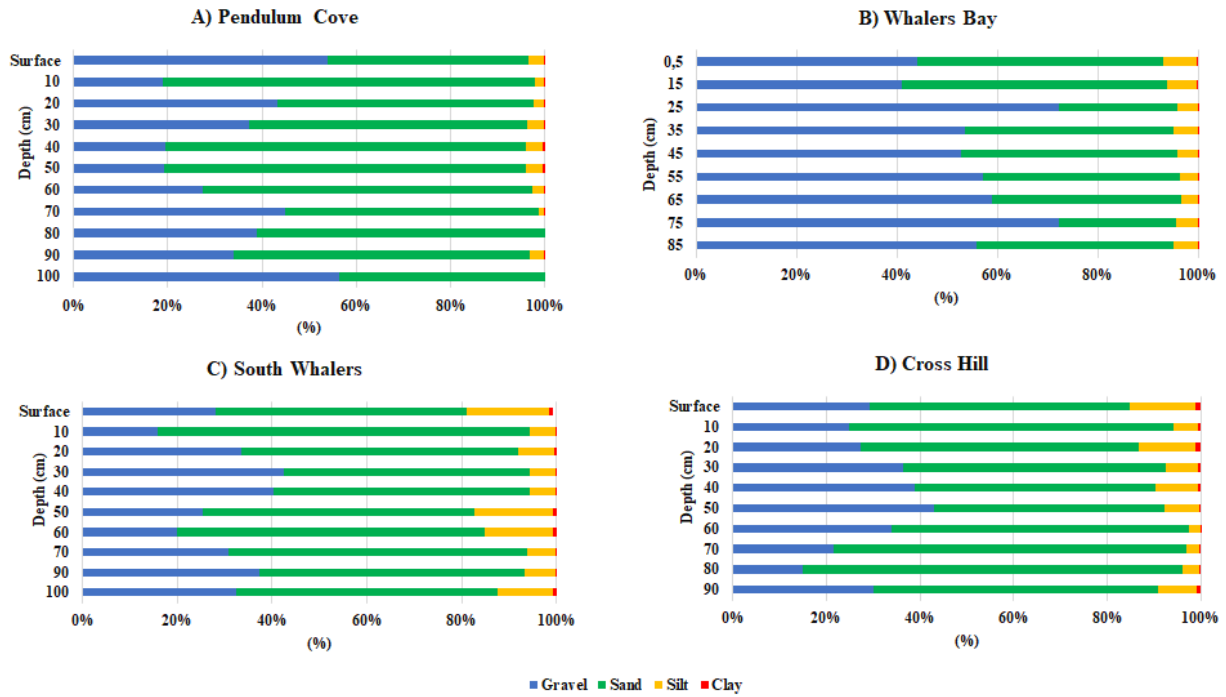


Figure 4. Particle size analysis of Pendulum Cove (A), Whalers Bay (B), South Whalers (C) and Cross Hill (D).

Figure 5 presents the morphoscopic characteristics of the profiles of Pendulum Cove, Whalers Bay, South Whalers and Cross Hill, where (VA) means very angular grains, (A) angular grains, (SA) subangular grains, (SR) sub-rounded grains, (R) rounded grains and (WR) well-rounded grains.

The sediment analysis at Pendulum Cove profile (100 cm deep) reveals distinct grain characteristics across different depths. At the surface and the 30, 40 and 50 cm layers, there is a noticeable prevalence of sub-rounded, rounded and well-rounded grains, suggesting some level of transport and weathering. In contrast, the 10, 20, 60, 70, 80, 90 and 100 cm layers predominantly feature very angular, angular and sub-angular grains. This disparity in grain shape indicates that those layers have undergone less transportation, likely reflecting more recent deposition processes.

Whalers Bay, South Whalers and Cross Hill exhibit a higher concentration of very angular, angular and subangular clasts throughout entire profiles (85, 100 and 90 cm deep, respectively). This pattern may indicate different processes involved in material transport, such as lower-energy transport over short distances. These results align with expectations for glacial environments where glacier friction and short distance prevent significant sediment rounding (EVANS; BENN, 2004).

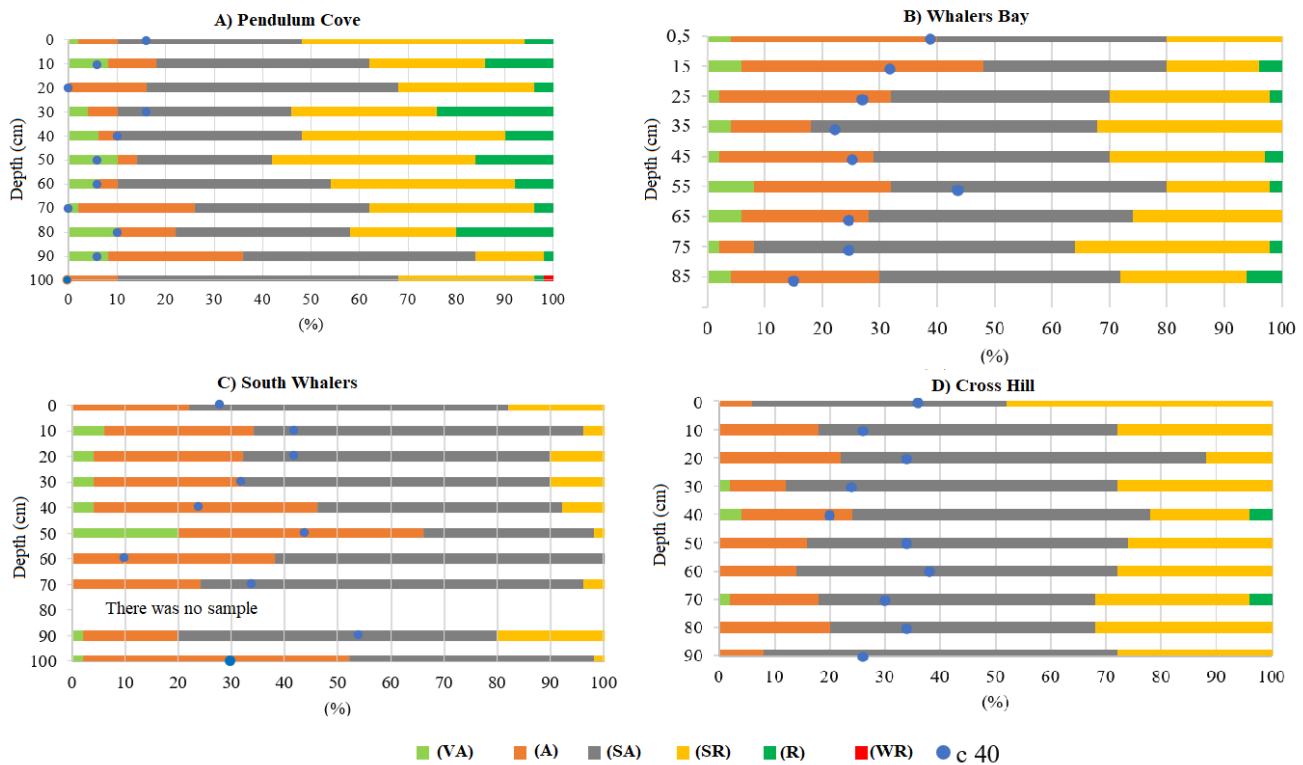


Figure 5. Profiles of Pendulum Cove (A), Whalers Bay (B), South Whalers (C) and Cross Hill (D) with their respective sample roundness data and C40 Index.

The analysis of the Pendulum Cove C40 index shows values ranging from 0 to 16%, which are considered low and indicate sediments with a higher degree of weathering. The lowest C40 values are found at the 10, 20, 50, 60, 70, 90, and 100 cm layers, with the 50 cm layer exhibiting the most rounded and weathered grains. Additionally, the lower C40 values compared to those of the other sites (Figure 5), can be attributed to the greater granulometric composition of the sand fraction, as observed in Figure 4.

The C40 index in Whalers Bay reaches its highest value at the 55 cm layer (42%), where the highest concentration of very angular, angular and sub-angular sediments is found, indicating a slightly weathered character for this layer. The other layers present values ranging from 18% (85 cm) to 38% (0.5 cm), denoting more weathered grains at depth and in the middle of the profile, while grains closer to the surface exhibit less weathering.

In South Whalers, the C40 index varies from low values (10% at the 60 cm layer) to intermediate values (54% at the 90 cm layer), revealing a profile with a mix of both more weathered grains (at the surface and in the 40 and 60 cm layers) and less weathered grains (in the 10, 20, 50, 70 and 90 cm layers).

Cross Hill's C40 index generally falls within an intermediate range, varying from 20% on the 40 cm layer to 38% on the 60 cm layer. The highest values—38% at the 60 cm layer, 36% at the surface, and 34% at the 20 cm, 50 cm, and 80 cm layers—indicate lower degrees of weathering. In contrast, the 40 cm (20%), 30 cm (24%), 10 cm (26%), and 90 cm (26%) layers exhibit a greater degree of weathering.

Figure 6 (A-B) illustrates the relationship between the C40-RA and C40-RWA indices across the Pendulum Cove, Whalers Bay, South Whalers and Cross Hill profiles. Pendulum Cove, similar to Whalers Bay, exhibits medium RA and RWR indices. Meanwhile, South Whalers and Cross Hill present medium and low values, respectively.

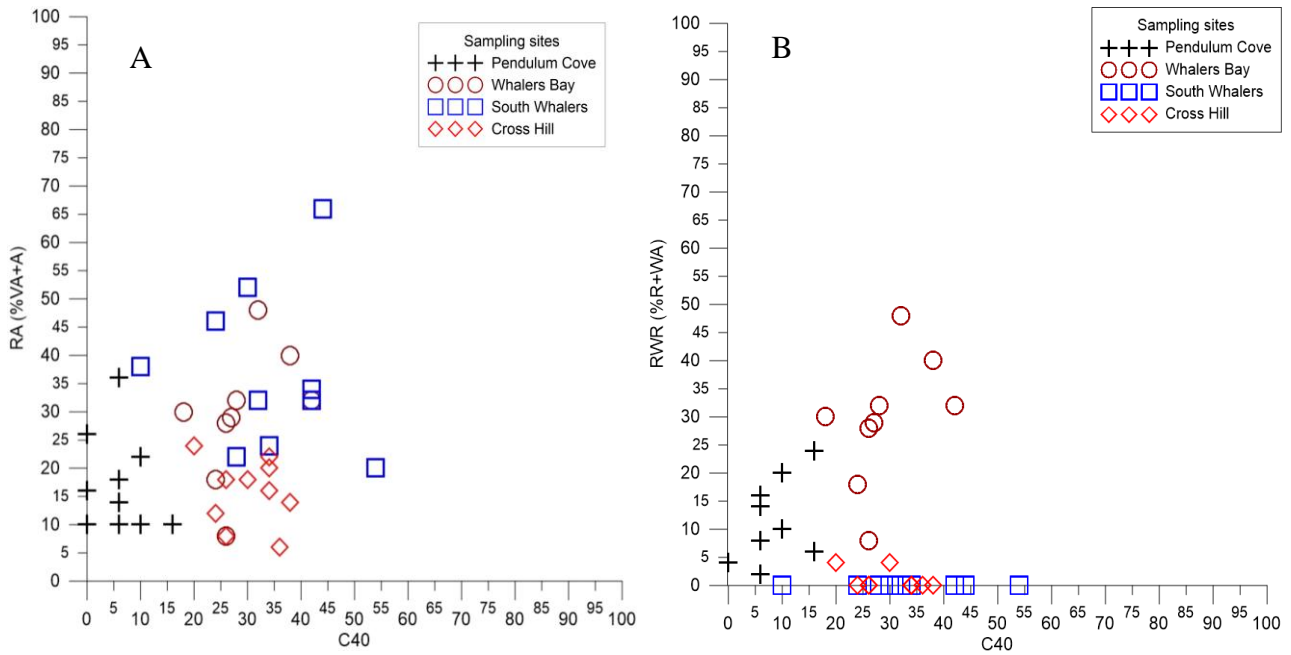
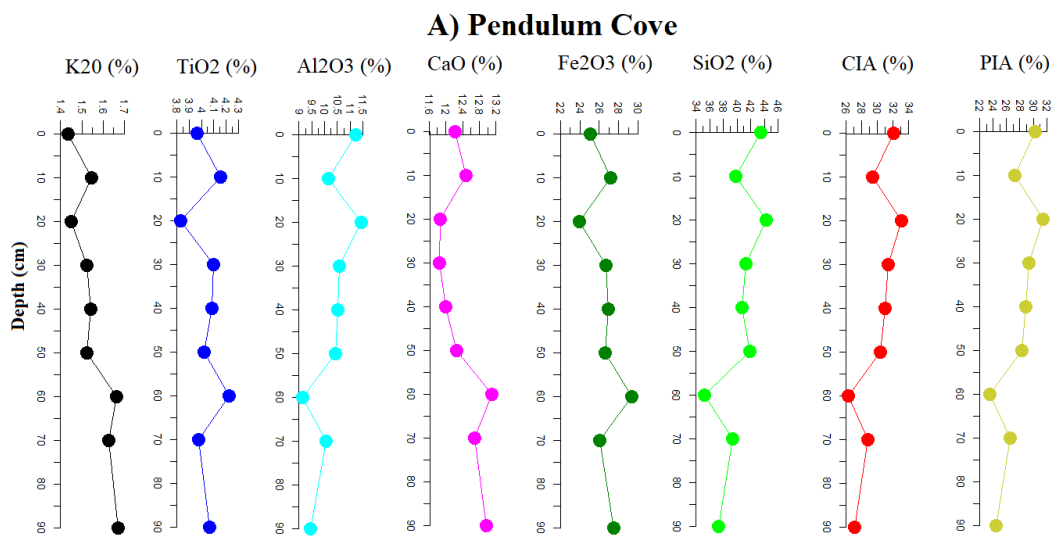


Figure 6. Diagrams of C40-RA (A) and C40-RWR (B).

When applying the C40-RA and C40-RWA indices (Figure 6A-B), which differentiate passively and actively transported clasts (BENN; BALLANTINE, 1994), the four sampling profiles exhibit low to medium C40, as well as medium RA and RWR values. It is important to note that the term “fluvial” in the context of Deception Island refers to meltwater flows, i.e. glaciofluvial processes.

4.2. Chemical elements and weathering

Figure 7 presents the percentage concentration of the main oxides found in samples from Pendulum Cove, Whalers Bay, South Whalers and Cross Hill, along with the values of the Chemical Alteration Index (CIA) and the Plagioclase Alteration Index (PIA).



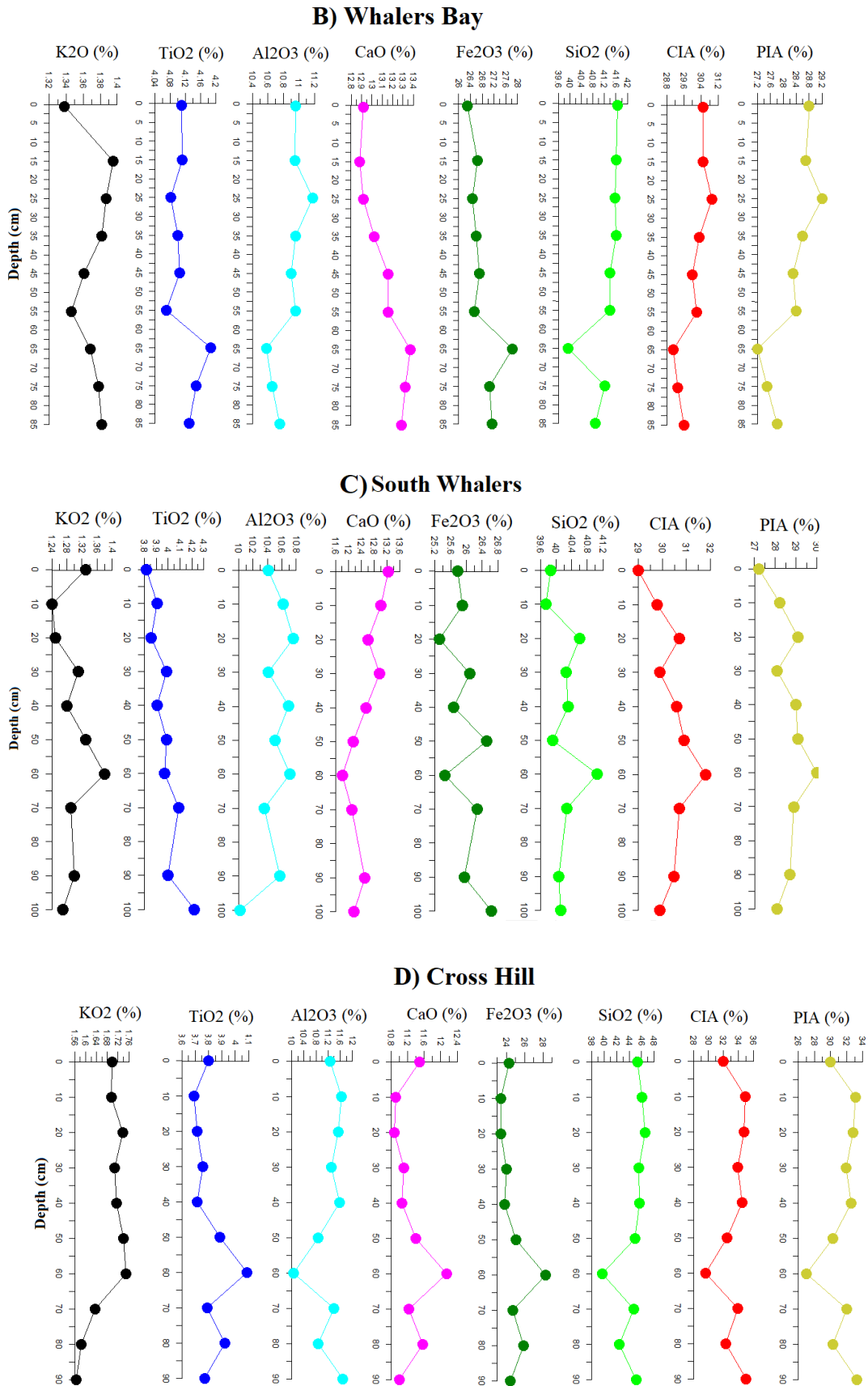


Figure 7. Profiles of Pendulum Cove (7A), Whalers Bay (7B), South Whalers (7C) and Cross Hill (7D) with their respective data on the concentration of the main oxides, Chemical Alteration Index and Plagioclase Alteration Index.

SiO₂ is the most abundant oxide across all four profiles, followed by Fe₂O₃, CaO, Al₂O₃, TiO₂ and K₂O, respectively. In Pendulum Cove, SiO₂ ranges from 35.2% (minimum value at the 60 cm layer) to 43.4% (maximum value at the surface). In Whalers Bay SiO₂ varies between 39.9% (minimum value at the 65 cm layer) to 41.7% (maximum at the 0.5 cm layer). In South Whalers, SiO₂ ranges from 39.7% (minimum value at the 10 cm layer) to 41% (maximum value at the 60 cm layer). In the Cross Hill profile, SiO₂ varies between 38.7% (minimum at the 60 cm layer) to 44.6% (maximum at the 20 cm layer).

Fe₂O₃ variation in the Pendulum Cove ranges from 23.9% (minimum concentration at the 20 cm layer) to 29.6% (maximum concentration at the 60 cm layer). In Whalers Bay, Fe₂O₃ varies from 26.2% (minimum at 0.5 cm layer) to 27.8% (maximum at the 65 cm layer). In South Whalers, Fe₂O₃ ranges between 25.3% (minimum value at the 20 cm layer) and 26.6% (maximum value at the 100 cm layer). In the Cross Hill profile, Fe₂O₃ varies from 22.4% (minimum value at the 20 cm layer) to 27.5% (maximum value at the 60 cm layer).

CaO in the Pendulum Cove profile ranges from 11.8% (minimum at the 30 cm layer) to 13.2% (maximum concentration at the 60 cm layer). In Whalers Bay, CaO varies from 12.8% (minimum value at the 15 cm layer) to 13.7% (maximum value at the 65 cm layer). In South Whalers, CaO varies between 11.8% (minimum value at the 60m cm layer) to 13.2% (maximum value on the surface). In the Cross Hill profile, CaO varies between 10.4% (minimum value at the 20 cm layer) to 11.8% (maximum value at the 60 cm layer).

In the Pendulum Cove profile, Al₂O₃ ranges from 9.1% (minimum at the 60 cm layer) to 11.2% (maximum at the surface). In Whalers Bay, Al₂O₃ varies between 10.5% (minimum at the 65 cm layer) and 11.1% (maximum at the 25 cm layer). In South Whalers, Al₂O₃ ranges from 10% (minimum at the 100 cm layer) to 10.8% (maximum at the 20 cm layer). In the Cross Hill profile, Al₂O₃ varies between 9.8% (minimum at the 60 cm layer) to 11.2% (maximum at the 90 cm layer).

The Pendulum Cove profile shows a variation of TiO₂, ranging from 3.8% (minimum concentration at the 20 cm layer) to 4.2% (maximum concentration at the 60 cm layer). In Whalers Bay, TiO₂ varies from 4.1% (minimum value at the 55 cm layer) to 4.2% (maximum value at the 65 cm layer). In South Whalers TiO₂ ranges from 3.8% (minimum value at the surface) to 4.2% (maximum value at the 100 cm layer). In the Cross Hill profile, TiO₂ varies between 3.6% (minimum value at the 10 cm layer) and 3.9% (maximum value at 60 cm layer).

K₂O in the Pendulum Cove profile ranges from 1.4% (minimum concentration at the surface) to 1.7% (maximum concentration at the 90 cm layer). In Whalers Bay, K₂O varies from 1.3% (minimum value at the 0.5 cm layer) to 1.4% (maximum value at the 15 cm layer). In South Whalers, K₂O ranges between 1.2% (minimum value at the 10 cm layer) to 13.2% (maximum value at the surface). In the Cross Hill profile, K₂O varies from 10.4% (minimum value at the 20 cm layer) to 1.4% (maximum value at the 60 cm layer).

The Chemical Index of Alteration (CIA) and Plagioclase Index of Alteration (PIA) values range between 26% and 35% at all sampling points. CIA and PIA values tend to decrease with increasing depth in the Pendulum Cove and Whalers Bay profiles. In the South Whalers profile (Figure 7C), however, the opposite trend is observed, with CIA values increasing as depth increases.

No clear trend is observed in the Cross Hill profile (Figure 16D) regarding the CIA, except for a sharp decrease at the 60 cm layer.

4.3. Isotope analysis

Figure 8 presents the results of the carbon isotopic analysis ($\delta^{13}\text{C}$) and amount of total organic carbon content for the profiles of Pendulum Cove, Whalers Bay, South Whalers and Cross Hill. There are no data for the 50 cm layer at Pendulum Cove and for the 20 cm and 60 cm layers at South Whalers. Furthermore, the analysis covers depths of up to 25 cm in Whalers Bay and 30 cm in Cross Hill.

The lack of data is due to incomplete carbon burning in these layers, resulting from the low organic matter content in the samples. The $\delta^{15}\text{N}$ and TN (total nitrogen) values were extremely low in the analyses and were disregarded in this study.

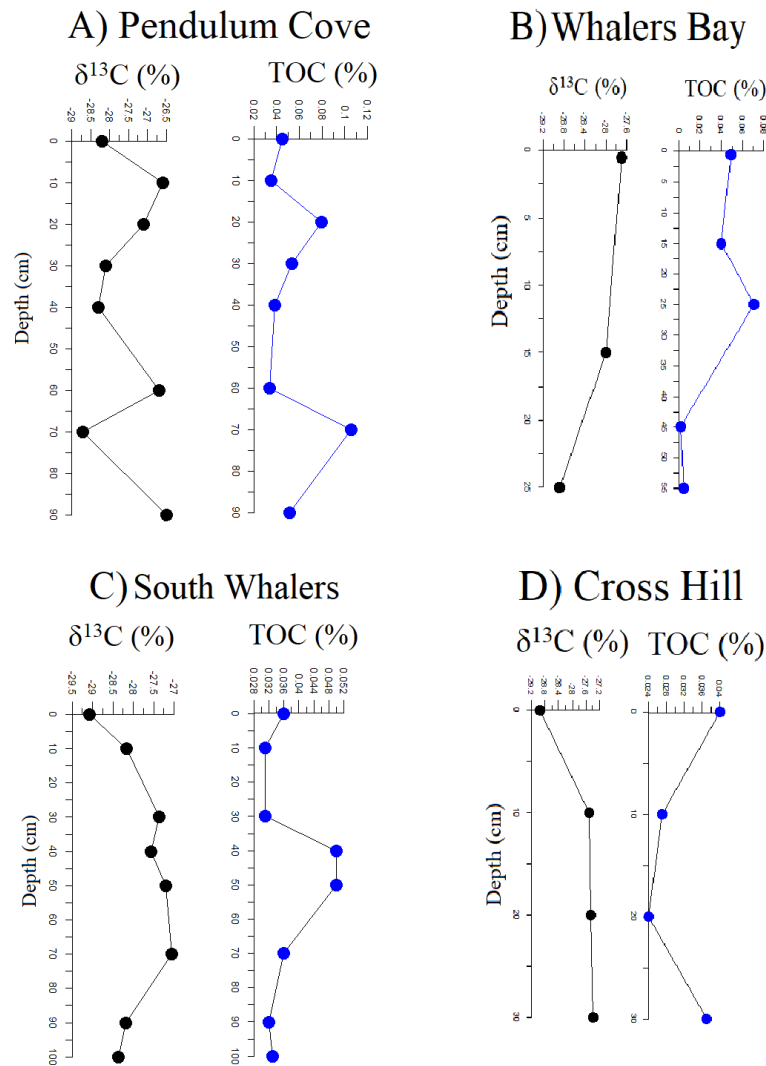


Figure 8. Carbon isotope analysis results and total carbon values for Pendulum Cove (A), Whalers Bay (B), South Whalers (C) and Cross Hill (D) profiles.

In the Pendulum Cove profile (Figure 8A) the total organic carbon (TOC) content decreases from the surface (0.04%) to the 10 cm layer (0.03%). At the 20 cm layer, an increase to 0.07% is observed, followed by a decline at 30 cm (0.05%), 40 cm (0.03%) and 60 cm (0.03%) layers. The 70 cm layer presents the highest organic matter content in the profile (0.1%), which then decreases again to the 90 cm layer (0.05%).

A variation in $\delta^{13}\text{C}$ values is observed, ranging from -28.7‰ at the 70 cm layer (the layer with the highest TOC content) to -26.5‰ at the 90 cm layer. From the surface to the 10 cm layer, $\delta^{13}\text{C}$ value show enrichment (-28.2‰ to -26.6‰). Beyond this point, a trend toward depletion is observed, with values decreasing from -26.6‰ at the 10 cm layer to -27.1‰ at the 20 cm layer, -28.1‰ at the 30 cm, and -28.3‰ at the 40 cm. At the 60 cm layer an enrichment occurs (-26.7‰), followed by depletion at the 70 cm layer (-28.7‰, lowest value in the profile), before enriches again at the 90 cm layer (-26.5‰).

In Whalers Bay (Figure 8B) TOC content tends to increase from the 0.5 cm layer (0.04%) to the 25 cm layer (0.07%). A decrease is observed from the 45 cm layer (0.001%) followed by a slight increase at the 55 cm layer (0.004%). Regarding $\delta^{13}\text{C}$ values, a depletion trend is observed in the upper 25 cm of the profile, from -27.7‰ at 0.5 cm to -28.0‰ at 15 cm and -28.9‰ in the 25 cm.

In the South Whalers profile (Figure 8C), the TOC value decreases from the surface (0.036%) to the 30 cm layer (0.032%). At the 40 cm and 50 cm layers, the value increases again (0.050% in both), but at the 70 cm and 100 cm layers, it decreases once more (0.036 % and 0.033%, respectively). A trend of $\delta^{13}\text{C}$ surface enrichment is observed,

from -29‰ at the surface to -27.3‰ at the 30 cm. At the 40 cm layer, the value shows a slight depletion (-27.4‰), followed by enrichment towards the 70 cm layer (-27‰). At the 100 cm layer, the $\delta^{13}\text{C}$ value decreases again to -28.3‰.

In the Cross Hill profile (Figure 8D) the TOC value decreases in the first three layers (from 0.040% at the surface to 0.027 at the 10 cm layer and 0.024% at the 20 cm layer) before increasing again at the 30 cm layer (0.037%). The $\delta^{13}\text{C}$ values show enrichment with depth, from -28.9‰ at the surface to -27.5‰ at the 10 cm layer, -27.4‰ at the 20 cm layer, and -27.3‰ at the 30 cm layer.

4.4. Statistical analysis

In the Pendulum Cove profile (Figure 9A), a relatively significant negative correlation is observed between CIA and layer depth. Depth correlates positively with Cl, K and K₂O and negatively with Al, Si, Al₂O₃ and SiO₂. Among the elements and oxides, the most significant positive correlations are found between CIA and Al, CIA and Si, and CIA and their respective oxides. The most significant negative correlations occur. Similarly with K, Cl, K₂O, CaO, TiO₂ and Fe₂O₃.

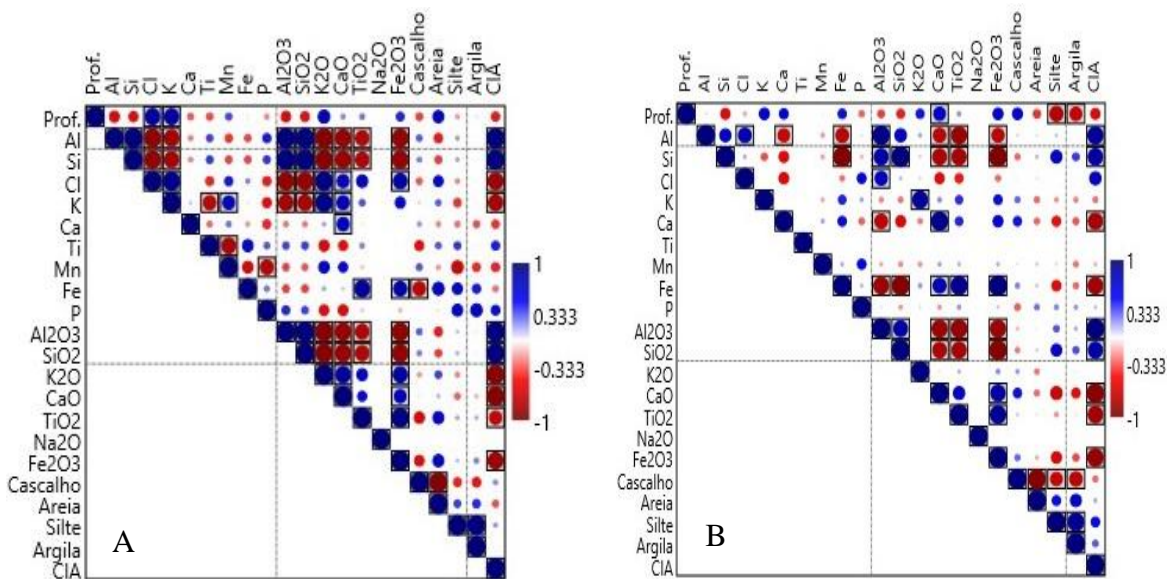
Similarly, in the Whalers Bay profile (Figure 9B) a relatively significant negative correlation is observed between CIA and layer depth. Depth is significantly correlated only to CaO (positive) and with K, Ca, Fe, K₂O, and Fe₂O₃. Significant correlations are also observed between CIA and Al, CIA and Si, CIA and Al₂O₃, and CIA and SiO₂ (positive), as well as between CIA and Ca, CIA and Fe, CIA and CaO, CIA and TiO₂ and CIA and Fe₂O₃ (negative).

In the South Whalers profile (Figure 9C) the correlation between CIA and depth is significantly positive. Depth also correlates positively with Ti and TiO₂, while it correlates negatively with Ca and CaO. CIA exhibits a positive correlation with Al and Al₂O₃ and a negative correlation with Ca and CaO.

In the Cross Hill profile (Figure 9D), layer depth shows a very weak correlation with CIA and weak correlations with elements and oxides. CIA correlates significantly positively with Al, Si, Al₂O₃, and SiO₂ while it correlates negatively with Ca, Mn, Fe, CaO, TiO₂, and Fe₂O₃.

Regarding grain size, depth shows a relatively significant positive correlation with the sand fraction only in Pendulum Cove and a relatively significant negative correlation only in Whalers Bay. The silt and clay fractions are significantly negatively correlated with depth in Whalers Bay and relatively negatively correlated in Cross Hill. In the other profiles, correlations between depth and particle size fractions are of low significance.

Correlations between CIA and particle size fractions are relatively significant and positive only with the silt fraction in Whalers Bay and Cross Hill and significantly positive with the clay fraction in Cross Hill.



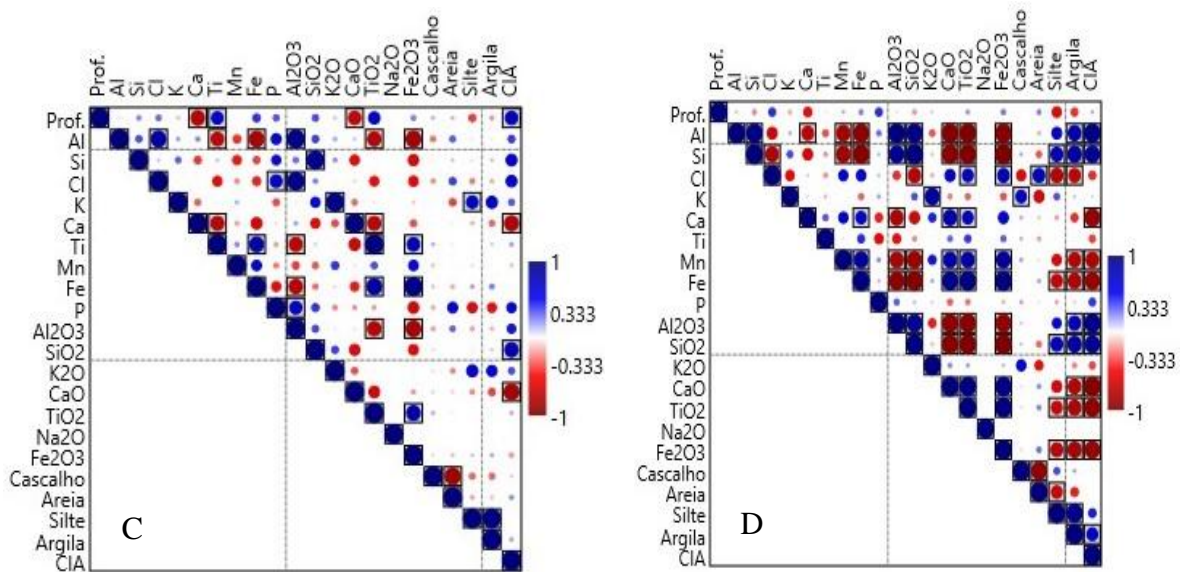


Figure 9. Pearson correlation between different variables analyzed from the points of Pendulum Cove (A), Whalers Bay (B), South Whalers (C) and Cross Hill (D). The most significant correlations are identified by filled squares. Correlations with less significance and possibility of correlation are not presented.

Applying Principal Component Analysis (PCA) to the elements and oxides of Pendulum Cove, Whalers Bay, South Whalers and Cross Hill, it is possible to identify the driving data variability processes (Figure 10A-D). In Pendulum Cove (10A and A') Component 1 explains 88.0% of the data variance, while Component 2 accounts for 9.8%. The highest scores correspond to the highest loading (A') of SiO₂/Si and Al₂O₃/Al (positive) and Cl and Fe₂O₃ (negative). This indicates in layers with higher percentages of SiO₂/Si and Al₂O₃/Al, the percentages of other elements and oxides are lower. The highest scores are associated with the 20 cm layer and the surface layer, while the lowest scores correspond to the 60 cm layer, where P has the lowest loading. The 30 cm, 40 cm and 50 cm layers exhibit similar scores. The 60 cm layer is distinct, as Component 2 (accounting for 9.8% of the variance), has its highest scores at a depth of 40 cm, with Fe and Mn showing high positive and negative loadings, respectively. The 70 cm layer presents the lowest score.

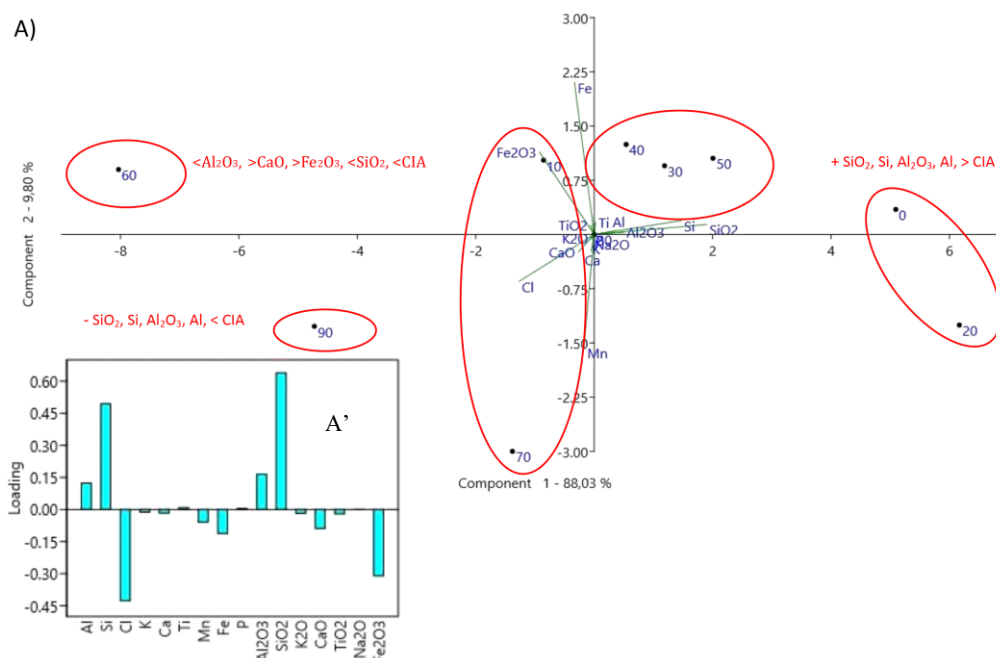


Figure 10. (A-A') Biplot shows the first two principal components of the PCA of the Pendulum Cove profile, together explaining 97.8% of the variance. The distribution of elements/oxides throughout the layers is identified. The length of the arrows indicates the degree of the influence of the environmental variables to the principal axes, such Fe, Si, Cl, SiO₂ and Fe₂O₃. The bar chart corresponds to Principal Component 1. The parts highlighted with ellipse correspond to the depths of the layers.

In Whalers Bay (11B-B') PC1 explains 92.7% of the variance, while PC2 accounts for 4.1%. The highest scores correspond to the highest loadings of Fe₂O₃/Fe and CaO and CaO/Ca (positive), and SiO₂/Si and Al₂O₃/Al (negative). The highest scores are associated with the 65 cm layer, where Fe₂O₃ and SiO₂ have the highest positive and negative loadings, respectively. The lowest scores correspond to the 45 cm layer, with P showing the lowest loading. Layers from 0.5 cm to 55 cm exhibit similar scores, while the 60 cm layer is distinct from the others. PC2, which explains 4.1% of the variance, has its highest scores at a depth of 75 cm, with Ca and Fe showing high positive loading. The 0.5 cm layer presents the lowest score with Ti having the lowest loading.

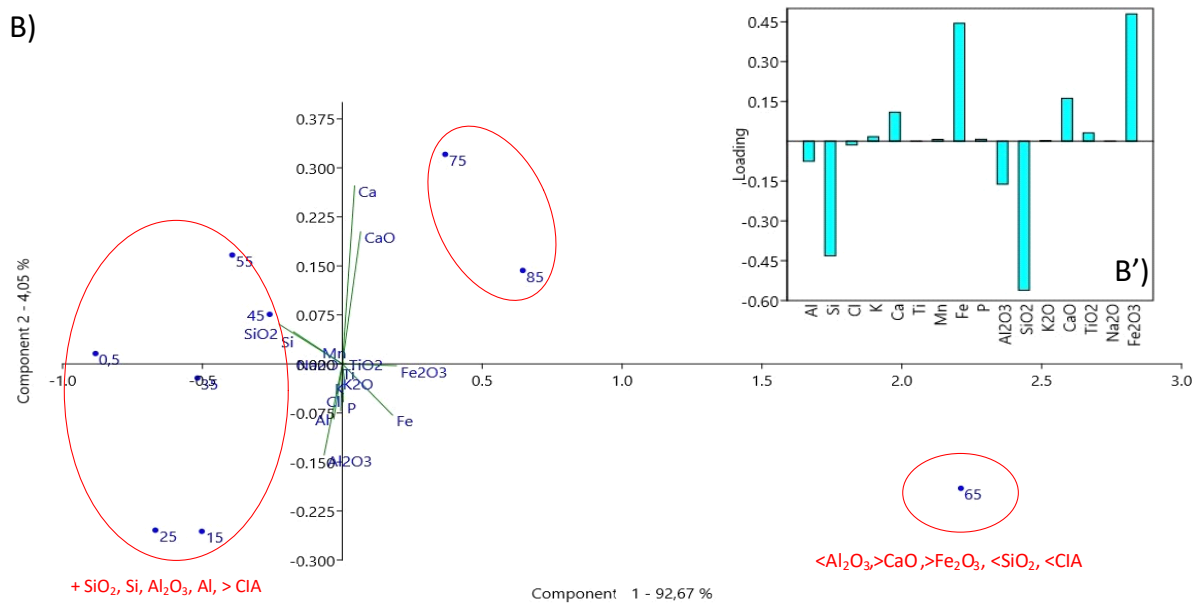


Figure 11. (B-B') Biplot shows the first two principal components of the PCA of the Whalers Bay profile, together explaining 96.8% of the variance. The distribution of elements/oxides throughout the layers is identified. The length of the arrows indicates the degree of the influence of the environmental variables to the principal axes, such Fe, Si, Ca, SiO₂ and CaO. The bar chart corresponds to Principal Component 1. The parts highlighted with ellipse correspond to the depths of the layers.

In South Whalers (12C-C') PC1 explains 56.2% of the variance, while PC2 accounts for 36.6%. The highest scores correspond to the highest loadings (C') of Ca/CaO and Al₂O₃/Al (positive), and Fe/Fe₂O₃ and Ti/TiO₂ (negative). The highest scores are associated with the surface layer and the 100 cm layer, while the lowest scores correspond to the 90 cm layer, where K₂O has the lowest loading. The 60 cm layer is distinct from the others. PC2, which explains 36.6% of the variance, has its highest scores at the depth of 20 cm (negative) and in the surface layer (positive), with SiO₂ and Fe₂O₃ showing the highest negative and positive loadings, respectively. The lowest scores correspond to depths of 40 and 90 cm, with Ti having the lowest loading.

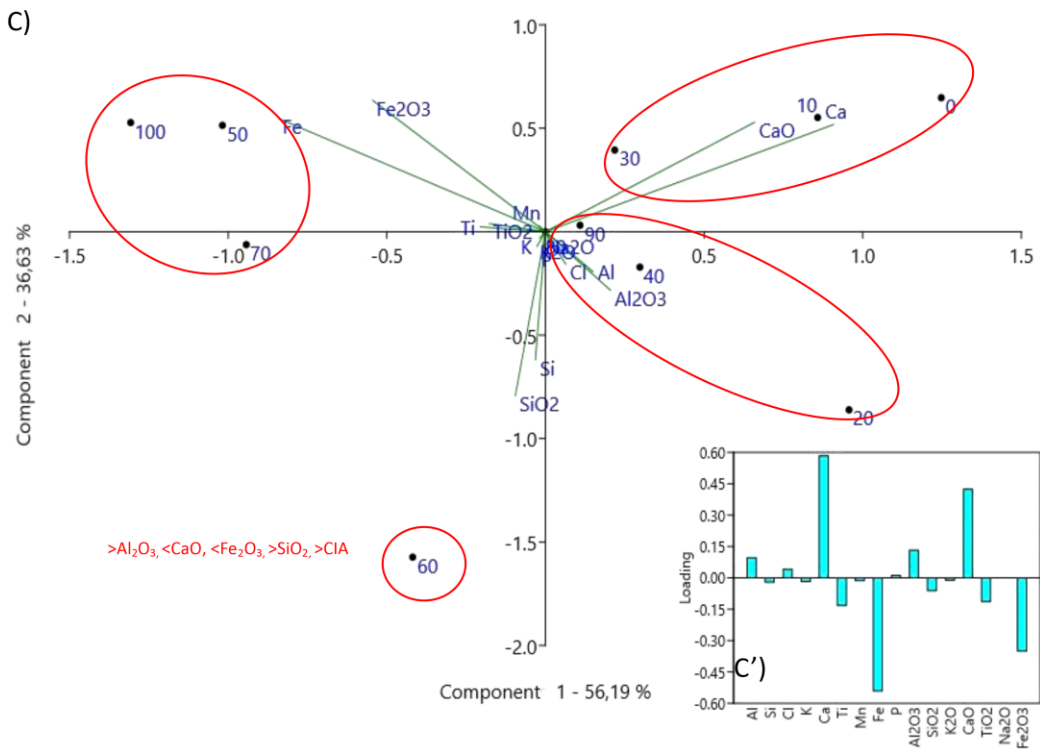


Figure 12. (C-C') Biplot shows the first two principal components of the PCA of the South Whalers profile, together explaining 98.8% of the variance. The distribution of elements/oxides throughout the layers is identified. The length of the arrows indicates the degree of the influence of the environmental variables to the principal axes, such Fe, Si, Ca, Fe₂O₃, SiO₂, CaO, and Al₂O₃. The bar chart corresponds to Principal Component 1. The parts highlighted with ellipse correspond to the depths of the layers.

In Cross Hill (13D-D'), PC1 explains 95.8% of the variance, while PC2 accounts for 3.2%. The highest scores correspond to the highest loadings (D') of SiO₂/Si and Al₂O₃/Al (positive), and Fe₂O₃/Fe and Cl (negative). The highest scores are associated with the 60 and 80 cm layers, while the lowest scores correspond to the 50 cm layer, where P has the lowest loading. PC2, which explains 3.2% of the variance, has the highest scores at a depth of 50 cm, with Cl and Fe showing high negative and positive loadings, respectively. The lowest scores occur at 90 cm, where P and Mn have the lowest loadings.

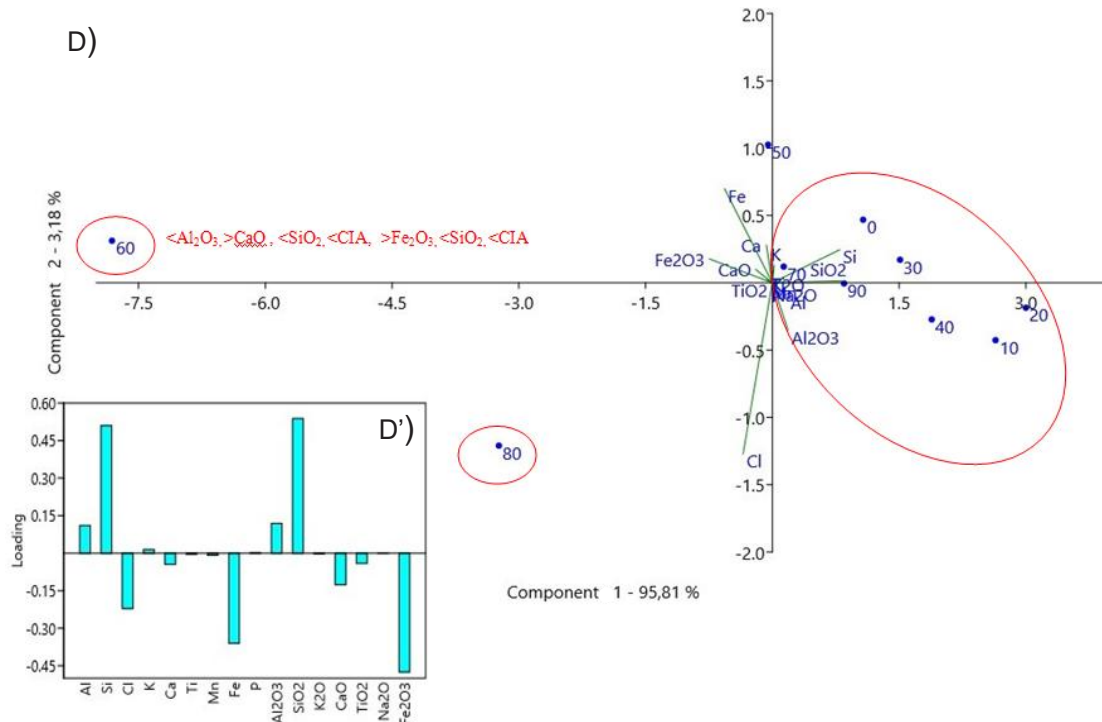


Figure 13. (D-D') Biplot shows the first two principal components of the PCA of the Cross Hill profile, together explaining 99% of the variance. The distribution of elements/oxides throughout the layers is identified. The length of the arrows indicates the degree of the influence of the environmental variables to the principal axes, such Fe, Si, Cl, Fe₂O₃ and SiO₂. The bar chart corresponds to Principal Component 1. The parts highlighted with ellipse correspond to the depths of the layers.

5. Discussion

5.1. Morphology and physical properties of profiles

5.1.1. Pendulum Cove

The high concentration of sand and gravel fractions supports the interpretation of a shorter transport and reworking distance from their source area, with fine fractions being transported to Porto Foster Bay. The analysis of the Pendulum Cove C40 Index shows values ranging from 0 and 16%, which are considered low and indicate sediments with a higher degree of weathering. The lowest C40 values are found at depths of 10, 20, 50, 60, 70, 90 and 100 cm, with the 50 cm layer exhibiting the most rounded and worn grains. Additionally, the lower C40 values, compared to those at other sites (Figure 5), can be attributed to the higher sand fraction content, as observed in Figure 4.

Applying the C40-RA and C40-RWA indices (Figure 6A-B), which differentiate passively and actively transported clasts (BENN; BALLANTINE, 1994), Pendulum Cove exhibits low C40, medium RA and medium RWR. According to the classification developed by Lukas et al. (2013), this suggests transport under subglacial to glaciofluvial conditions. It is important to note that Deception Island the term “fluvial” as refers to meltwater flows, i.e. glaciofluvial processes.

According to Smellie (2001) and the geomorphological map by López-Martínez; Serrano (2002), the sediments sampled in Pendulum Cove are alluvial deposits resulting from volcanic eruptions in the 19th century (1829, 1839 and 1842) and in 1969, forming the Pendulum Cove Formation. As described by Tostes (2011), the Pendulum Cove Formation is part of the Monte Pond Group, which corresponds to the post-caldera phase.

5.1.2. Whalers Bay

Whalers Bay exhibits a higher concentration of clasts throughout its entire profile (85 cm deep) within the very angular, angular, and subangular fractions. The high concentration of sand and gravel fractions supports the interpretation of a shorter transport and reworking distance of sediments from their source area. The C40 index reaches its highest value at the 55 cm layer (42%), where the greatest concentration of very angular, angular and subangular sediments is observed, indicating a slightly weathered character for this layer. The remaining layers present values ranging from 18% (85 cm layer) to 38% (0.5 cm layer), suggesting more weathered grains in depth and the middle of the profile, with less-worn grains close to the surface.

The clasts exhibit medium C40, medium RA and medium RWR, also indicating subglacial to glaciofluvial transport conditions (Figure 6A-B).

It can therefore be inferred that the surface material collected in Whalers Bay consists of post-caldera alluvial deposits from the Pendulum Cove Formation, originating from the mountains surrounding the coastline (SMELLIE, 2001). According to the geological map (LÓPEZ-MARTÍNEZ; SERRANO, 2002), the highest sector of the area is occupied by moraine deposits.

5.1.3. South Whalers

The area surrounding the sampling point contains both pre- and post-caldera deposits (LÓPEZ-MARTÍNEZ; SERRANO, 2002), as well as the presence of glaciers. Similar to Whalers Bay, South Whalers presents a higher concentration of clasts throughout their entire profile (100 cm depth) within the very angular, angular and subangular fractions. This suggests that the sediments in the profile were transported with less energy or over relatively short distances. The high concentration of sand and gravel fractions further supports the interpretation of a shorter transport and reworking distance from their source area. The C40 index varies from low values (10% at the 60 cm layer) to intermediate values (54% at the 90 cm layer), indicating a mixture of both more weathered grains (surface, 40 and 60 cm layers) and less weathered grains (10 cm, 20 cm, 50 cm, 70 cm and 90 cm layers). According to the diagrams in Figure 6A-B, the clasts are influenced by subglacial to glaciofluvial processes.

The material collected at South Whalers consists of alluvial deposits, which may originate from the Pendulum Cove or Fumarole Bay formation, located in the mountains surrounding the coastline (SMELLIE, 2001; MUNIZ et al., 2018). It is also important to consider the presence of glaciers at higher elevations and near the coastal sectors.

5.1.4. Cross Hill

The sampling areas are located near the coastline, where the presence of permafrost is not recorded (VIEIRA et al., 2008). The excavation of 1-meter-deep trenches at the four sampling sites confirms this characteristic. The sampling point is situated on flat terrain with a dark gray surface, surrounded by elevated areas and post-caldera deposits. During the eruptions between 1967 and 1970, fissures opened between Goddard Hill and Cross Hill, forming various types of craters due to the interaction of lava with the water-saturated ground, glaciers and seawater (GEYER et al., 2021).

The Cross Hill profile (90 cm deep) also shows a predominance of clasts within the very angular, angular and subangular fractions throughout its depth. As observed in the other profiles, this indicates sediment transport over short distances. The high concentration of sand and gravel fractions further supports the interpretation of a shorter transport and reworking distance from their source area. The C40 index exhibits moderate values, ranging from 20% in the 40 cm layer to 38% in the 60 cm layer. The highest values found in the 60 cm layer (38%), surface layer (36%) and 20 cm (34%), 50 cm (34%) and 80 cm (34%) layers, indicate lower degrees of weathering. In contrast, the 40 cm (20%), 30 cm (24%), 10 cm (26%) and 90 cm (26%) layers show a higher degree of weathering. The RA and RWR indices present medium and low values, respectively, indicating transport influenced by water flow.

Permafrost and volcanic material cover the slopes surrounding the sampling areas, acting as thermal insulation (VIEIRA et al., 2008). The sedimentary cover in higher-altitude sectors is thinner due to the slope gradient, whereas in lower areas, the sediment thickness increases due to the accumulation of material eroded from higher elevations. This transport has been intensified by meltwater flows, and permafrost degradation has already been identified on slopes and in lower valleys. In areas with gentler slopes, material transfer occurs at a lower intensity, contributing less to the sediment supply in coastal areas, as noted by Vieira et al. (2008). Coarser-

grained sediments (gravels) tend to accumulate in the lower sectors of the slopes. However, part of this material is likely transported to the coastal zone during more intense meltwater flows events originating from glaciers, snowdrifts, and permafrost. Additionally, the increase in liquid precipitation over recent decades may be altering geomorphic dynamics, enhancing sediment transfer from slopes to coastal areas (BOCKHEIM et al., 2013).

5.2. Chemical elements, granulometry and weathering

Chemical weathering intensifies under humid conditions, particularly in unstable minerals such as feldspar, leading to the loss of Na, K and Ca. In contrast, less soluble residual products, such as Al and Si, can reorganize into new minerals (e.g., clay minerals, Si and Al oxides), which tend to concentrate in the finer-grained fractions (FEDO et al., 1995; LEPSCH, 2011). However, local factors must also be considered, including lithology, slope position, aspect and thickness of the regolith, and the variability of wet and dry conditions (DIXON; THORN, 2005).

As shown in Figure 4, sand is the dominant particle size fraction in the analyzed profiles, followed by gravel. However, the silt and clay fractions provide key insights into chemical weathering processes (DARMODY et al., 1987). In glacial environments sand is typically produced subglacially through crushing processes, whereas silt and clay result from abrasion (HALDORSEN, 1981). Fine-grained fractions, such as silt and clay, are abundant in subglacial till but can be transported and redistributed by wind or glaciofluvial flows. Additionally, the presence of volcanic deposits can be covers and altered from non-volcanic sediment source, making it more difficult to differentiate their contribution (LICHT; HEMMING, 2017).

The presence of heated soils, fumaroles and hot springs illustrates the hydrothermal activity in the Whalers Bay sector, which was affected by a jokulhlaup during the 1969 eruption. This event incorporated meltwater from snow and ice, forming a lahar deposit (LÓPEZ-MARTÍNEZ; SERRANO, 2002). A 4 km-long fissure opened between Whalers Bay and Pendulun Cove, beneath the Mount Pond glacier, releasing large volumes of subglacial meltwater (PEDRAZI et al., 2018).

In Pendulum Cove (Figure 7A) and Whalers Bay (Figure 7B), lower CIA and PIA values at increasing depth correspond to higher concentration of K and Cl and K₂O, along with lower concentrations of Al, Si, Al₂O₃ and SiO₂. Additionally, fine-grained fractions decrease with depth, particularly in Whalers Bay, indicating more intense chemical weathering in layers up to 60 cm in Pendulum Cove and 65 cm in Whalers Bay. In South Whalers (Figure 7C), CIA values increase up to 60 cm, coinciding with higher SiO₂ and Si concentrations, which represent less soluble residues. At Cross Hill (Figure 7D), CIA values remain relatively stable up to 40 cm but reach a minimum at 60 cm. These chemical weathering indices suggest an early stage of chemical weathering but provide insight into past geomorphic processes on the island and their chronology.

The decline in CIA and PIA values with depth, reaching minimums at 60 cm in Pendulum Cove and Cross Hill, 65 cm in Whalers Bay, and 70 cm in South Whalers, suggests immature terrain conditions at these depths, likely linked to rapid or more intense sedimentation events. Principal Component Analysis (Figures 10-13) supports this interpretation by distinguishing these layers from the rest of the profiles.

The distribution of Fe in the fine-grained fractions does not follow a consistent pattern. In Pendulum Cove, Fe content increases alongside silt and clay fractions. Conversely, in Whalers Bay and Cross Hill, Fe and Fe₂O₃ concentrations decrease as silt and clay fractions increase. These variations may be related to water-rock interaction in the hydrothermal system, which contributes to the formation of clay minerals. It was not possible to conduct mineralogical analysis of the sediments, which would have provided further insight into the mineral composition.

5.3. Carbon isotope analysis

The organic material found in coastal profiles can have two main types of sources, autochthonous and allochthonous. Autochthonous organic material comes from in situ sources, such as organic matter that grows on the surface. Allochthonous organic material, in turn, is transported from other regions by erosive agents such as tidal currents, wind, ice, meltwater channels, and liquid precipitation (ESTEVEZ et al., 2011).

The $\delta^{13}\text{C}$ values in the analyzed profiles (Figure 8) overlap with those found for C3 Antarctic plants, such as lichens (-28.1‰ to -18.8‰), as well as excrement from Antarctic animals (-30‰ to -25‰). It is important to note that C4 type tree plants and C3 land plants are not found in Maritime Antarctica. Therefore, the $\delta^{13}\text{C}$ values in the profiles indicate that the organic matter in the sediments is predominantly composed of terrestrial vegetation remains, more specifically lichens and/or excrement from Antarctic animals (LIU et al., 2005; 2006; 2016; CIPRO et al., 2011; MUNIZ et al., 2018).

At the Whalers Bay and South Whalers sampling points, no native vegetation was found (MUNIZ et al., 2018), suggesting that the organic material comes from allochthonous sources, transported by erosion. In Pendulum Cove, small patches of lichens and mosses were identified at the sampling point, indicating that the profile may contain a mixture of both autochthonous and allochthonous sources.

Therefore, it can be inferred that in addition to mosses and lichens, the profiles may also contain excrement from Antarctic birds, such as penguin guano. However, as discussed by Liu et al. (2006), isolated $\delta^{13}\text{C}$ values are not sufficient to conclusively confirm the presence of guano in these profiles. A correlation between the $\delta^{13}\text{C}$ and $\delta^{15}\text{N}$ values would be necessary, but this was not possible in this study.

The surface of Pendulum Cove profile (Figure 8A) presents total organic carbon (TOC) concentration equal to those of the surface of the Cross Hill profile. Additionally, the Pendulum Cove and Whalers Bay profiles (Figure 8B) have similar TOC concentrations in the first 25 cm of their profiles. However, in deeper layers, from 40 to 55 cm, the TOC values in the Pendulum Cove increase.

From the 60 cm layer to the 70 cm layer in Pendulum Cove, a significant increase in the TOC content is observed. According to Rumpel and Kogelknaber (2011), this could indicate the presence of carbonized organic material, which may have originated from past volcanic activities. At the 90 cm layer, the TOC value drops again, showing more stable values similar to the rest of the profile.

It is important to note that in the 60 cm layer of Pendulum Cove, the lowest percentage of TOC and enriched $\delta^{13}\text{C}$ are observed, suggesting low biological activity. The same pattern is observed in South Whalers at the 70 cm layer. This observation aligns with other variables highlighted in these layers, as seen in the correlation charts (Figure 9) and principal component analysis (Figures 10-13).

Considering that around 5 kyr BP the South Shetland region, and consequently Deception Island, was already undergoing a deglaciation process (INGÓLFSSON et al., 2008; SIMMS et al., 2011; COFAIGH et al., 2014; OLIVA et al., 2023), and that the sediments in the first 42 cm of the profiles analyzed by Muniz et al. (2018) have been dated to up to 10 kyr BP, it may be inferred that the organic matter in the deeper sediments of the sampling points in this study could be from periods even older than 10 kyr BP. However, the exact age cannot be estimated with certainty due to the lack of samples dating.

5.4. Glacial and volcanic activity

As noted by Lopes-Martinez; Serrano (2002), the non-recovery of glacier extension can be attributed not only to climatic events, such as negative mass balances (ORHEIN, 1972), but also to the volcanic activity itself during this period. The volcanic activity triggered a severe jokulhlaup in Whalers Bay in 1969.

Possible ancient morainic deposits from the pre-caldera period may have been destroyed or covered by volcanic flows, with their material likely mixed during these flows. This suggests that the sedimentation process was primarily controlled by volcanic activity between 1967 and 1970, with contributions from glacial and periglacial processes such as meltwater flows and sediments from glaciers and permafrost. These processes helped form fluvio-glacial deposits in the area, corroborating the findings of Lopes-Martinez; Serrano (2002).

The intensity of volcanic explosions led to the transport of sediment towards Porto Foster Bay from lahars and debris flows, likely activated by the intense and sudden heating of snow and glacial ice (SMELLIE, 2002). Fine-grained material was transported and deposited on the bay's bottom, as evidenced by muddy sand deposits

covering much of the seafloor of Porto Foster Bay (FINGER; LIPPS, 1981; COSTA et al., 2023). Gray et al. (2003), who analyzed marine (Porto Foster Bay) and subaerial (Pendulum Cove, Whalers Bay, and Cross Hill) sediments, noted changes in the granulometry of the beach sediments (gravelly sand), consistent with the granulometry observed in this study. They also reported slightly sand mud in the marine sediments.

Muniz et al. (2018), through radiocarbon dating, analysis of C and N isotopic composition, and particle size distribution along 50 cm soil profiles from Whalers Bay and Cross Hill, identified intense sedimentation activity and alteration of layers in the first 27 ± 2.5 cm. From this depth, from 27 cm to 50 cm, they observed greater stability in organic matter accumulation. The calculated age for the superficial 27 ± 2.5 cm layer to the 50 cm depth ranged from 5 to 13 cal kyr BP. Therefore, from 5 cal kyr BP to the present, post-caldera eruptions occurred, melting glaciers and permafrost, producing everything from surface flows with mud to lahars, and consequently altering the layers from 27 ± 2.5 cm to the surface.

The profiles analyzed in this work reached depths of 100 cm deep in Pendulum Cove and South Whalers, 90 cm in Cross Hill, and 85 cm in Whalers Bay. Given the ages reported by Muniz et al. (2018), the layers in these profiles may contain information from phases prior to the caldera collapse. The period between 10 kyr and 3,3 kyr BP, as suggested by other authors (ANTONIADES et al., 2018), as well as the early stages of the deglaciation process in the area, could be represented in these profiles.

Reconstructions of changes in the Antarctic Peninsula ice sheet, which extended over the Bransfield Strait and the South Shetland Islands during the Last Glacial Maximum (COFAIGH et al., 2014), show that Deception Island was covered by the ice sheet at 15 kyr BP but already disconnected from it at 10 kyr BP. At this time much of the South Shetland Islands and part of the Strait of Bransfield remained ice-covered. By 5 kyr BP, both the South Shetland Islands and Deception Island were undergoing deglaciation.

5. Conclusion

The particle size analysis reveals a predominance of sand and gravel fractions across all four sampling points, with a noticeable reduction in the silt and clay fractions. Additionally, the morphoscopic analysis shows a predominance of very angular, angular and subangular sediments in Whalers Bay, South Whalers and Cross Hill, while Pendulum Cove displays a mixture of angular and rounded grains. These characteristics suggest a short transport and reworking distance from the source area, coupled with rapid sedimentation of particles, possibly linked to hydrovolcanic eruptions in the case of Pendulum Cove.

In Pendulum Cove and Whalers Bay, the lower CIA and PIA indices in the upper layers, with increasing depth, correspond to higher values of K, Cl and K_2O , and lower values of Al, Si, Al_2O_3 and SiO_2 . This pattern is also supported by statistical analysis. In contrast, South Whalers shows the highest CIA values up to 60 cm, which correlate with higher concentrations of Al, Si, Al_2O_3 and SiO_2 . This indicates the intensification of chemical weathering processes, which result in the loss of Na, K, and Ca and an increase in Al and Si concentration in the sediments. Iron (Fe) is the predominant element in the profiles, exhibiting a negative correlation with the CIA index in Whalers Bay and Cross Hill, which may be linked to water-rock interaction in the hydrothermal system that produces ferromagnesian clay minerals.

Stable carbon isotopes analysis indicates that the organic matter in the profiles is primarily derived of plants such as lichens, possibly mixed with animal excrement from animals that live in the region. Further analysis using stable nitrogen isotopes would be necessary to confirm this presence of animal-derived organic material. Pendulum Cove may contain a mixture of allochthonous and autochthonous organic sources, while in Whalers Bay and South Whalers, the lack of native vegetation suggests that the organic matter is predominantly allochthonous, deposited by sediment transport processes.

The current sedimentation dynamics of Deception Island are mainly controlled by the volcanic activities of the 1967-1970 period. However, glacial and periglacial processes, including meltwater flows, liquid precipitation and sediment contributions from glaciers and permafrost, have also played an important role in forming glacio-fluvial deposits in the area. Despite this, the analysis points to older events that may alter sedimentation processes, particularly between the 60 and 70 cm layers in the four study areas, underscoring the need for further dating to fully understand the temporal dynamics of the region.

Authors Contributions: Conceptualization, R.V., D.P.; methodology, D.P., R.V., V.C. and J.F.; software, D.P. and R.V.; formal analysis, D.P., V.C., J.F. and R.V.; investigation, D.P., V.C. and R.V.; data preparation, D.P. and J.F.; writing—original draft, D.P., and R.V.; review and editing, D.P., V.C., J.F. and R.V.; supervision, R.V. All authors have read and agreed to the published version of the manuscript.

Funding: This research was funded by the National Council for Scientific and Technological Development (CNPq) and Brazilian Antarctic Program (PROANTAR), process n° 407598/2013-8 (expedition and laboratory equipment), and by Fundação Carlos Chagas Filho de Amparo à Pesquisa do Estado do Rio de Janeiro, process n° E-26/210.510/2019 (laboratory equipment)

Acknowledgments: We thank the reviewers of this article for their contributions, as well the Brazilian Antarctic Program and INCT of Cryosphere for providing the infrastructure for the development of this research.

Conflicts of Interest: The authors declare no conflicts of interest.

References

1. ABNT – Associação Brasileira de Normas Técnicas. **NBR 6.502 – Rochas e solos: terminologia**. Rio de Janeiro: ABNT. 18 p, 1995.
2. ABRAM, N.J., MULVANEY, R. WOLFF, E.W., TRIEST, J., KIPFSTUHL, S., TRUSEL, L.D. Acceleration of snow melt in an Antarctic Peninsula ice core during the twentieth century. **Nature Geoscience**, n.6, p. 1-8, 2013. DOI: 10.1038/ngeo1787.
3. ANTONIADES, D., GIRALT, S., GEYER, A., ÁLVAREZ-VALERO, A.M., PLA-RABES, S., GRANADOS, I., LIU, E.J., TORO, M., SMELLIE, J.L., OLIVA, M. The timing and widespread effects of the largest Holocene volcanic eruption in Antarctica. **Scientific Reports**, v. 8, n. 17279, 2018.
4. APARICIO, A., RISSO, C. VIRAMONTE, J.G., MENEGATTI, N., PETRINOVIC, L. El volcanismo de isla Deception (Península Antártica). **Boletín Geológico y Minero**, p. 235-258, 1997.
5. BALDWIN, R.J., SMITH JR., K.L. Temporal dynamics of particulate matter fluxes and sedimentation unity response in Port Foster, Deception Island, Antarctica. *Deep Sea Research Part II Top. Stud. Oceanography*, 50, p. 1707-1725. 2003.
6. BALLANTYNE, C.K. Paraglacial geomorphology. **Quaternary Science Reviews** 21, p. 1935-2017, 2002.
7. BARALDO, A., RINALDI, C.A. Stratigraphy and structure of Deception Island, South Shetland Islands, Antarctica. **Journal of South American Earth Sciences**, v. 13, n. 8, p. 785-796, 2000.
8. BARTOLINI, S., GEYER, A., MARTÍ, J., PEDEAZZI, D., AGUIRRE-DÍAZ, G. Volcanic hazard on Deception Island, Southern Shetland Islands, Antarctica. **Journal of Volcanology and Geothermal Research**, n. 285, p. 150-168, 2014. DOI: 10.1016/j.jvolgeores.2014.08.009.
9. BENN, D.I., BALLANTYNE, C.K. Reconstructing the transport history of glacial sediments: a new approach based on the covariance of clast form indices. **Sedimentary Geology**, n. 91, p. 215-227, 1994.
10. BLOTT, S.J., PYE, K. GRADISTAT: A grain size distribution and statistics package for the analysis of unconsolidated sediments. **Earth Surface Processes and Landforms**, v. 26, n. 11, p. 1237-1248, 2001. DOI: 10.1002/esp.261.
11. BOCKHEIM, J.; VIEIRA, G.; RAMOS, M.; LÓPEZ-MARTÍNEZ, J.; SERRANO, E.; GUGLIELMIN, M.; WILHELM, K.; NIEUWENDAM, A. Climate warming and permafrost dynamics in the Antarctic Peninsula region. **Global And Planetary Change**, p. 215-223, 2013. DOI: 10.1016/j.gloplacha.2012.10.018.
12. CARVALHO-SILVA, M., ROSA, L. H., PINTO, O. H.B., SILVA, T. H., HENRIQUES, D. K., CONVEY, P., CÂMARA, P. E.A. Exploring the plant environmental DNA diversity in soil from two sites on Deception Island (Antarctica, South Shetland Islands) using metabarcoding. **Antarctic Science**, p. 469-478, 2021. DOI: 10.1017/s0954102021000274.
13. CIPRO, C.V.Z., YOGUI, G.T., BUSTAMANTE, P., TANIGUCHI, S., SERICANO, J.L., MONTONE, R. C. Organic pollutants and their correlation with stable isotopes in vegetation from King George Island, Antarctica. **Chemosphere**, n. 85, p. 393-398, 2011.
14. COFAIGH, C.Ó., DAVIES, B.J., LIVINGSTONE, S.J. *et al.* Reconstruction of ice-sheet changes in the Antarctic Peninsula since Last Glacial Maximum. **Quaternary Science Review**, n. 100, p. 87-110, 2014.
15. CLARKE, A., HARRIS, C.M. Polar marine ecosystems: major threats and future change. **Environmental Conservation**, v. 30, n. 1, 2003.

16. COSTA, V., PORTELLA, D.A., VIEIRA, R., AYRES NETO, A. Diferenciação de ambientes de sedimentação glaciais e vulcânicos na ilha Deception (Arquipélago Shetland do Sul, Antártica) **Revista Brasileira de Geomorfologia**, v. 24, n. 3, p. 1-17, 2023. DOI: 10.20502/rbg.v24i3.2274
17. DALZIEL, I.W.D. Tectonic evolution of a forearc terrane, southern Scotia Ridge, Antarctica I.W.D. Dalziel (Ed.), Tectonic Evolution of a Forearc Terrane, Southern Scotia Ridge, Antarctica, 200, **Geological Society of America** 1984.
18. DARMODY, R.G., THORN, C.E., RISSING, J.M. Chemical weathering of fine debris from a series of Holocene moraines: Storbreen, Jotunheimen, southern Norway. **Geografiska Annaler**, n. 69, p. 405-413, 1987.
19. DIXON, J.C., THORN, C.E. Chemical weathering and landscape development in mid-latitude alpine environments. **Geomorphology**, n. 67, p. 127-145, 2005.
20. ESTEVES, F. D. A.; AMADO, A. M. **Fundamentos de Limnologia**. Rio de Janeiro: Interciência, Cap. 13, 2011. p. 239-258.
21. EUROPEAN SPACIAL AGENCY. **ESA Copernicus** online, 2023. Disponível em: <https://www.copernicus.eu/pt/node/1260>. Acesso em: 18 abril 2023.
22. EVANS, D., BENN, D. **A Practical Guide to the Study of Glacial Sediments**. London: Edward Arnold, 266 p. 2004.
23. FOOD AND AGRICULTURE ORGANIZATION. **Guidelines for soil description**. 4 ed. Rome: FAO, 2006. 97 p.
24. FEDO, C.M., NESBITT, H.W., YOUNG, G.M. Unraveling the effects of potassium metasomatism in sedimentary rocks and paleosols, with implications for paleo weathering conditions and provenance. **Geology**, v. 23, n. 10. p. 921-924, 1995.
25. FERREIRA, P., GUIMARÃES, F. CALDEIRA, R., MÃO DE FERRO, A., CANÁRIO, J. Química mineral das rochaspiroclásticas da ilha Deception (PenínsulaAntártica): algumas considerações petrogenéticas. **Comunicações Geológicas**, 102, Especial I, p. 11- 22. 2015.
26. FINGER, K.L., LIPPS, J.H. Foraminiferal decimation and repopulation in an active volcanic caldera, Deception Island, Antarctica. **Micropaleontology**, v. 27, n. 2, p. 111-139, 1981.
27. FOLK, R.L., WARD, W. Brazos river bar: a study in the significance of grain size parameters. **Journal of Sedimentary Petrology**, n. 27, p. 3-26, 1957.
28. GALVÃO, J.C.M. **Caracterização geoquímica e mineralógica de sedimentos marinhos e sua relação com os processos sedimentares e oceanográficos na Baía central de Bransfield – Antártica**. Dissertação (Mestrado Dinâmica dos Oceanos e da Terra) - Instituto de Geociências, Universidade Federal Fluminense, Niterói, 2021.143p.
29. GEYER, A., MARTI, A., GIRALT, S., FOLCH, A. Potential ash impact from Antarctic volcanoes: insights from Deception Island most recent eruption. **Scientific Reports**, n.7, p. 1-10, 2017. DOI: 10.1038/s41598-017-16630-9.
30. GEYER, A., PEDRAZZI, D., ALMENDROS, J., BERROCOSO, M., LÓPEZ-MARTÍNEZ, J., MAESTRO, A., CARMONA, E., ÁLVAREZ-VALERO, A.M., DE GIL, A. Volcanism in Antarctica: 200 Million Years of Subduction, Rifting and Continental Break-up. **Geological Society**, n. 55, p. 667-693, 2021.
31. GIBBS, M.M. **Protocols on the use of Compound-Specific Stable Isotope to identify and apportion soil source from land use**. Joint FAO/IAEA Division of Nuclear Techniques in Food and Agriculture, 103 p., 2010.
32. GOYANES, G., VIEIRA, G., CASELLI, A., CARDOSO, M., MARMY, A., SANTOS, F., BERNARDO, I., HAUCK, C. Local influences of geothermal anomalies on permafrost distribution in an active volcanic island, Deception Island, Antarctica. **Geomorphology**, 225, p. 57-68. 2014.
33. GRACIA, E., CANALS, M., FARREEN, M., PRIETO, M.J., SORBIDAS, J., PALIA, R. Central and Eastern Bransfield Basins, Antarctica, from a high resolution swath bathymetric data. **Antarctic Science**, v. 9, n. 2, p. 168-180, 1997.
34. GRAY, S.C., STURZ, A., BRUNS, M.D., MARZAN, R.L., DOUGHERTY, D., LAW, H.B., BRACKETT, J.E., MARCOU, M. Composition and distribution of sediments and benthic foraminifera in a submerged caldera after 30 years of volcanic quiescence. **Deep-Sea Research**, n. 50, p. 1727-1751, 2003.
35. HAMMER, O. **Paleontological Statistics version 2.16**. Manual de Referência, 2012. <http://folk.uio.no/ohammer/past/>.
36. HALDORSEN, S. Grain-size distribution of subglacial till and its relation to glacial crushing and abrasion. **Boreas**, n. 10, p. 91-105, 1981.

37. HOPFENBLATT, J., GEYER, A., AULINAS, M., ÁLVAREZ-VALERO, A.M., SÁNCHEZ, A.P., GIRALT, S., SMELLIE, J.L. DecTephra: A new database of Deception Island's tephra record (Antarctica). **Journal of Volcanology and Geothermal Research** v. 425, p. 107516, 2022.
38. HUBBARD, B., GLASSER, N. **Field Techniques in Glaciology and Glacial Geomorphology**. Oxford, John Wiley & Sons Ltd. 400 p. 2005.
39. INGÓLFSSON, Ó., HJORT, C., BJÖRCK, S., & SMITH, R. I. L. Late Pleistocene and Holocene glacial history of James Ross Island, Antarctic Peninsula. **Boreas**, P. 209–222, 2008. DOI:10.1111/j.1502-3885.1992.tb00029.x.
40. IPCC. Disponível em < <https://www.ipcc.ch/report/ar6/wg1/> > Acesso em dezembro/2022.
41. KELLER, R.A., FISK, M.R., SMELLIE, J.L., STRELIN, J.A., LAWVER, L.A. Geochemistry of back arc basin volcanism in Bransfield Strait, Antarctica: Subducted contributions and along-axis variations. **Journal of Geophysical Research: Solid Earth**, 107(B8), ECV-4. 2002.
42. LANDIN, P.M.B. **Análise Estatística de Dados Geológicos Multivariados**. Oficina de Textos, São Paulo, 208 p, 2011.
43. LEITÃO, F.J., AYRES NETO, A., VIEIRA, R. Morphological and sedimentar characterization through analysis of multibeam data at Deception Island, Antarctica. **Revista Brasileira de Geofísica**, v.34, n 2, p. 1-10, 2016.
44. LEPSCH, I.F. **Lições de Pedologia**. Oficina de Texto, São Paulo, 2011. 456p.
45. LICHT, K.J., HEMMING, S.R. Analysis of Antarctic provenance sediment provenance through geochemical and petrologic application. **Quaternary Science Reviews**, n. 164, p. 1-24, 2017.
46. LIU, X.D., SUN, L.G., XIE, Z.Q., YIN, X.B., WANG, Y.H. A 1300-year record of penguin populations on Ardley Island in Antarctica, as deduced from the geochemical data in the ornithogenic lake sediments. **Arctic, Antarctic and Alpine Research**, n. 37, p. 490-498, 2005.
47. LIU, X.D., LI, H.C., SUN, L.G., YIN, X.B., ZHAO, S.P., WANG, Y.H. $\delta^{13}C$ and $\delta^{15}N$ in the ornithogenic sediments from the Antarctic maritime as palaeoecological proxies during the past 2000 yr. **Earth and Planetary Science Letters**, n. 243, p. 424-438, 2006.
48. LIU, E.J., OLIVA, M., ANTONIADES, D., GIRALT, S., GRANADOS, I., PLA-RABES, S., TORO, M., GEYER, A. Expanding the tephro stratigraphical framework for the south Shetland Islands, Antarctica, by combining compositional and textural tephra characterisation. **Sedimentary Geology**, p. 49-61, 2016.
49. LÓPEZ-MARTÍNEZ, J., SERRANO, E. Geology and Geomorphology of Deception Island, 1:25 000. BAS GEOMAP Series Sheets 6-A and 6-B. British Antarctic Survey, Cambridge, UK, p. 31-39, 2002.
50. LUKAS, S., et al. Clast shape analysis and clast transport paths in glacial environments: a critical review of methods and the role of lithology. **Earth-Science Reviews**, n. 121, p. 96-116, 2013.
51. MAESTRO, A., SOMOZA, L., REY, J., MARTÍNEZ-FRÍAS, J. LÓPEZ-MARTÍNEZ, J. Active tectonics, fault patterns, and stress field of Deception Island: A response to oblique convergence between the Pacific and Antarctic plates. **Journal of South American Earth Sciences**, n. 23, p. 256-268, 2007.
52. MUNIZ, M.C., ANJOS, R.M., CARDOSO, R.P., ROSA, L.H., VIEIRA, R., MAROTTA, H., MACARIO, K., AYRES NETO, A., FELIZARDO, J.P., BARBOZA, C.D.N. Post-caldera evolution of Deception Island (Bransfield Strait, Antarctica) over Holocene timescales. **Palaeogeography, Palaeoclimatology, Palaeoecology**, n.501, p. 58-69, 2018. DOI: 10.1016/j.palaeo.2018.04.010.
53. NESBITT, H.W., YOUNG, G.M. Early Proterozoic climates and plate motions inferred from major element chemistry of lutites. **Nature**, n. 299, p. 715-717, 1982.
54. OLIVA, M.; PALACIOS, D.; FERNÁNDEZ-FERNÁNDEZ, J. M.; FERNANDES, M.; SCHIMMELPFENNIG, I.; VIEIRA, G.; ANTONIADES, D.; PÉREZ-ALBERTI, A.; GARCÍA-OTÉYZA, J. Holocene deglaciation of the northern Fildes Peninsula, King George Island, Antarctica. **Land Degradation & Development**, p. 3973-3990, 2023. Wiley. DOI: 0.1002/ldr.4730.
55. ORHEIM, O. **A 200-year record of glacier mass balance at Deception Island, Southern Atlantic Ocean and its bearing on models of global climatic change**. Institute of Polar Studies, Ohio, 1972. 118 p.
56. PEDRAZZI, D., NÉMETH, K., GEYER, A., ÁLVAREZ-VALERO, A.M., AGUIRRE-DÍAZ, G., BARTOLINI, S. Historic hydrovolcanism at Deception Island (Antarctica): implications for eruption hazards. **Bulletin of Volcanology**, n. 80, p. 1-28, 2018. DOI: 10.1007/s00445-017-1186-9.

57. PRESS, W.H., TEUKOLSKY, S.A., VETTERLINE, W.T., FLANNERY, B.P. **Numerical Recipes**. Cambridge University Press. 1992. DOI: 10.1017/SO269964800000565
58. RUMPEL, C., KOGEL-KNABNER, I. Deep soil organic matter - a key but poorly understood component of terrestrial C cycle. **Plant Soil**, n. 338, p. 143-158, 2011.
59. SIMMS, A. R.; MILLIKEN, K. T.; ANDERSON, J. B.; WELLNER, J. S. The marine record of deglaciation of the South Shetland Islands, Antarctica since the Last Glacial Maximum. **Quaternary Science Reviews**, v. 30, p. 1583-1601, 2011. DOI: 10.1016/j.quascirev.2011.03.018.
60. SMELLIE, J.L. Lithostratigraphy and volcanic evolution of Deception Island, South Shetland Islands. **Antarctic Science**, n. 13, p. 188-209, 2001.
61. SMELLIE, J.L. The 1969 subglacial eruption on Deception Island (Antarctica): events and processes during an eruption beneath a thin glacier and implications for volcanic hazards. **Geological Society**, London, Special Publications, 2002.
62. SMELLIE, J.L., LÓPEZ-MARTÍNEZ, J. Geological and geomorphological evolution: summary. In: López-Martínez, J., Smellie, J.L., Thomson, J.W., Thomson, M.R.A. (eds.). *Geology and geomorphology of Deception Island*, Cambridge, **British Antarctic Survey**, p. 54-57, 2002.
63. SVENDSEN, H., BEZCZYNSKA, A., LAFAUCCONNIER, B., TVERBERGV, V., GERLAND, S., HAGEN, J., ORBEAK, O., BISCHOF, J.B., PAPUCCI, C., ZAJACZKOWSKI, M., AZZOLINI, R., BRULAND, O., WIENCKE, C., WHINTHER, J.G., HODSON, A., MUMFORD, P. The physical environment of Kongsfjorden-Krossfjorden: – an Arctic fjord system in Svalbard. **Polar Research**, v. 21, 2002.
64. TOSTES, J.O. **Solos e Paisagens do Setor Oeste da Ilha Deception, Antártica Marítima**. Dissertação (Mestrado em Agronomia) - Instituto de Agronomia, Universidade Federal Rural do Rio de Janeiro, Itaguaí. 2011. 112p.
65. TURNER, J., BARRAND, N.E., BRACEGIRDLE, T.J. et al. Antarctic climate change and the environment: an update. **Polar Record**, v.50, n. 3, p. 237-259, 2014. DOI: 10.1017/S0032247413000296.
66. VIEIRA, G., LOPEZ-MARTINEZ, J., SERRANO, E., RAMOS, M., GRUBER, S., HAUCK, C., BLANCO, J.J. Geomorphological observations of permafrost and ground-ice degradation on Deception and Livingston islands, Maritime Antarctica. In: **9th International Conference on Permafrost**, Fairbanks, Alaska. p. 1840-1844, 2008.



Esta obra está licenciada com uma Licença Creative Commons Atribuição 4.0 Internacional (<http://creativecommons.org/licenses/by/4.0/>) – CC BY. Esta licença permite que outros distribuam, remixem, adaptem e criem a partir do seu trabalho, mesmo para fins comerciais, desde que lhe atribuam o devido crédito pela criação original.